

1  
2  
3  
4  
5  
6  
7  
8  
9  
10  
11  
12  
13  
14  
15  
16  
17  
18  
19  
20  
21  
22  
23  
24  
25  
26  
27  
28  
29  
30  
31  
32  
33  
34

**Maf/ham1-like pyrophosphatases of non-canonical nucleotides are host-specific partners of viral RNA-dependent RNA polymerases**

Adrian A. Valli<sup>1, \*</sup>, Rafael García López<sup>1</sup>, María Ribaya<sup>1, ¶</sup>, Francisco Javier Martínez<sup>1</sup>,  
Diego García Gómez<sup>2</sup>, Beatriz García<sup>1</sup>, Irene Gonzalo<sup>1</sup>, Alfonso Gonzalez de Prádena<sup>1</sup>,  
Fabio Pasin<sup>1, §</sup>, Inmaculada Montanuy<sup>3</sup>, Encarnación Rodríguez-Gonzalo<sup>2</sup>, Juan Antonio  
García<sup>1</sup>.

<sup>1</sup>Centro Nacional de Biotecnología (CNB-CSIC), Madrid, 28049, Spain

<sup>2</sup>Departamento de Química Analítica, Nutrición y Bromatología, Universidad de Salamanca, Salamanca, 37008, Spain

<sup>3</sup>Facultad de Ciencias Experimentales, Universidad Francisco de Vitoria, Madrid, 28223, Spain

\*Correspondence: Adrian A. Valli, [avalli@cnb.csic.es](mailto:avalli@cnb.csic.es)

Current addresses

<sup>¶</sup>Centre for Research in Agricultural Genomics (CRAG-CSIC-IRTA-UAB-UB), Cerdanyola del Vallès, Barcelona, 08193, Spain.

<sup>§</sup>Instituto de Biología Molecular y Celular de Plantas (IBMCP, UPV-CSIC), Valencia, 46022, Spain

## 35 **Abstract**

36 Cassava brown streak disease (CBSD), dubbed the “Ebola of plants”, is a serious threat  
37 to food security in Africa caused by two viruses of the family *Potyviridae*: cassava  
38 brown streak virus (CBSV) and Ugandan (U)CBSV. Intriguingly, U/CBSV, along with  
39 another member of this family and one secoviridae, are the only known RNA viruses  
40 encoding a protein of the Maf/ham1-like family, a group of widespread  
41 pyrophosphatase of non-canonical nucleotides (ITPase) expressed by all living  
42 organisms. Despite the socio-economic impact of CBSD, the relevance and role of this  
43 atypical viral factor has not been yet established. Here, using an infectious cDNA clone  
44 and reverse genetics, we demonstrate that UCBSV requires the ITPase activity for  
45 infectivity in cassava, but not in the model plant *Nicotiana benthamiana*. HPLC-  
46 MS/MS experiments showed that, quite likely, this host-specific constraint is due to an  
47 unexpected high concentration of non-canonical nucleotides in cassava. Finally, protein  
48 analyses and experimental evolution of mutant viruses indicated that keeping a fraction  
49 of the yielded UCBSV ITPase covalently bound to the viral RNA-dependent RNA  
50 polymerase (RdRP) optimizes viral fitness, and this seems to be a feature shared by the  
51 other members of the *Potyviridae* family expressing Maf/ham1-like proteins. All in all,  
52 our work (i) reveals that the over-accumulation of non-canonical nucleotides in the host  
53 might have a key role in antiviral defense, and (ii) provides the first example of an  
54 RdRP-ITPase partnership, reinforcing the idea that RNA viruses are incredibly versatile  
55 at adaptation to different host setups.

56

## 57 **Keywords**

58 RNA virus; virus/host coevolution; RNA-dependent RNA polymerase; RdRP; plant  
59 defence; ITP; XTP; Euphorbiaceae; *Potyviridae*; Ipomovirus.

60

## 61 **Introduction**

62 The family *Potyviridae* is the largest and most socio-economically relevant group of  
63 plant-infecting RNA viruses. With more than 200 assigned members sorted in 12  
64 different genera, these viruses represent a major threat for basically every important  
65 crop on earth. Potyvirids (members of the family *Potyviridae*) share common features,  
66 such as (i) monopartite (except for a few bipartite viruses) and positive sense single-  
67 stranded RNA (+ssRNA) genome, (ii) transmission mediated by vectors, and (iii)  
68 picorna-like gene expression strategy based on large polyproteins further processed by

69 viral-encoded proteinases (Revers and García, 2015, Yang et al., 2021, Valli et al.,  
70 2021). Potyvirids, in most cases, produce 10 mature proteins: P1, HCPro, P3, P3N-  
71 PIPO, 6K1, CI, 6K2, NIa (VPg/NIaPro), NIb and CP. Of relevance to this study, NIaPro  
72 is a *cis*- and *trans*-acting proteinase that releases most of the mature factors from the  
73 polyprotein (Carrington and Dougherty, 1987a, Carrington and Dougherty, 1987b), and  
74 NIb is a RNA-dependent RNA polymerase (RdRP) that replicates the viral genome  
75 (Allison et al., 1986, Hong and Hunt, 1996).

76 With seven members described so far, the *Ipomovirus* genus is the most versatile group  
77 of potyvirids in term of genome organization, since only two of them follow the most  
78 common arrangement mentioned above (Dombrovsky et al., 2014). The remaining five  
79 ipomoviruses lack the HCPro coding region and express either one P1 proteinase or two  
80 P1s in tandem (Valli et al., 2006, Valli et al., 2007, Mbanzibwa et al., 2009). Two  
81 viruses infecting *Manihot esculenta* (cassava) in nature are classified in this genus:  
82 cassava brown streak virus (CBSV) and Ugandan cassava brown streak virus (UCBSV),  
83 which cause the devastating cassava brown streak disease (CBSD), also dubbed the  
84 “Ebola of plants” (Patil et al., 2015, Tomlinson et al., 2018). Indeed, CBSD is  
85 considered among the seven most detrimental plant diseases in the world for its impact  
86 on the economy and food security in Africa, where it causes about 750 million US\$  
87 annual losses just in Tanzania, Uganda, Kenya and Malawi (Pennisi, 2010, Hillocks and  
88 Maruthi, 2015).

89 Even though CBSV and UCBSV are two distinct viral species, their genomes share  
90 around 72% nucleotide sequence identity, just below the species demarcation criteria in  
91 potyvirids (76%) (Winter et al., 2010). Moreover, these two viruses (i) encode a single  
92 P1 leader proteinase, (ii) lack HCPro and, as the most striking feature, (iii) present an  
93 extra cistron between NIb and CP that encodes a *bona fide* Maf/Ham1-like protein  
94 (Mbanzibwa et al., 2009). This protein (referred as HAM1 in this study) belongs to the  
95 inosine triphosphate (ITP) pyrophosphatase (ITPase) family, which hydrolyzes the  
96 pyrophosphate bonds in triphosphate substrates (ITP/XTP) to release the corresponding  
97 monophosphate (IMP/XMP) and a pyrophosphate molecule (Hwang et al., 1999, Lin et  
98 al., 2001, Chung et al., 2001, Chung et al., 2002). The presence of putative cleavage  
99 sites for the NIaPro proteinase at the N- and C-termini of HAM1 suggested that this  
100 protein accumulates into infected cells as a free product (Mbanzibwa et al., 2009).

101 HAM1-like enzymes are present in prokaryotes and eukaryotes, across all life  
102 kingdoms, where they are proposed to prevent (i) incorporation of non-canonical

103 nucleotides into nascent DNA and RNA molecules, (ii) RNA mistranslation, and (iii)  
104 inhibition of ATP-dependent enzymes (Simone et al., 2013). Although they are  
105 widespread in nature, HAM1-like proteins are not usually encoded in viral genomes; in  
106 fact, their presence has been reported in only four RNA viruses so far. Intriguingly, all  
107 these HAM1-expressing RNA viruses infect plants from the *Euphorbiaceae* family:  
108 three potyvirids [CBSV, UCSBV and euphorbia ringspot virus (EuRV, *Potyvirus*  
109 genus)] (Mbanzibwa et al., 2009, Knierim et al., 2017), and one virus from the  
110 *Secoviridae* family [cassava torrado-like virus (CsTLV)] (Jiménez Polo et al., 2018).  
111 Even though a recent study has shown that CBSV and UCBS HAM1s are genuine  
112 pyrophosphatases in *in vitro* experiments, and that they determine necrotic symptoms in  
113 the model plant *Nicotiana benthamiana* (Tomlinson et al., 2019), relevance and defined  
114 role of viral-derived HAM1 proteins are still unknown.

115 In this study, among other approaches, we used reverse genetics to manipulate an  
116 infectious cDNA clone of UCBSV in order to gain insight about the role of RNA virus-  
117 derived HAM1 proteins. Briefly, our experiments revealed that: (i) HAM1 is required  
118 for the virus to infect cassava, but not to produce a successful infection in the model  
119 plant *N. benthamiana*, and (ii) it works in partnership with the viral RdRP. The  
120 extremely high levels of non-canonical nucleotides that we have found in cassava, and  
121 likely present in other *Euphorbiaceae* plants, should have worked as a strong selection  
122 pressure to promote the acquisition of an ITP/XTP pyrophosphatase activity into virus  
123 RdRP in order to support successful replication and infection.

124

## 125 **Material and Methods**

126 **Plants.** Cassava plants were grown in a chamber with 16h/8h light/dark cycles at 28°C.  
127 *N. benthamiana* plants were grown in a greenhouse with 16h/8h light/dark cycles at 20-  
128 to-24°C with supplementary light. For viral infection, *N. benthamiana* plants were  
129 moved just after inoculation to the cassava-growing chamber.

130

131 **Plasmids.** Oligonucleotides used for this study are listed in Supplementary table S1.  
132 UCBSV full-length clones derive from pLX-UCBSVi, a version of pLX-UCBSV  
133 (GenBank KY825157.1) (Pasin et al., 2017) that carries the second intron of *Solanum*  
134 *tuberosum* ST-LS1 gene to interrupt the UCBSV P3 cistron. To generate pLX-UCBSVi,  
135 the mentioned intron was first amplified by PCR from pIC-PPV (Lopez-Moya and  
136 Garcia, 2000) with primers #3257/#3258. The 3'-half part of the UCBSV P3 cistron

137 was amplified by PCR with primers #3259/#3260. An overlapping PCR with primers  
138 #3257/#3260 was used to join these two PCR products [intron-P3(3'half)]. UCBSV P1  
139 and the 5'-half part of the UCBSV P3 cistron [P1-P3(5'-half)] were amplified with  
140 primers #3255/#3256. Finally, a DNA fragment that carries P1-P3(5'-half)-intron-  
141 P3(3'half) was produced by overlapping PCR with primers #3255/#3260, using P1-  
142 P3(5'-half) and intron-P3(3'half) as templates. This PCR product was digested with  
143 Bsu36I and NheI and introduced by ligation in pLX-UCBSV, which had been digested  
144 with the same enzymes, to replace the equivalent intron-less DNA segment.

145 To generate pLX-UCBSVi-eGFP (a GFP-tagged version of UCBSV), pLX-UCBSVi  
146 was used as backbone to introduce the GFP coding sequence between the HAM1 and  
147 CP cistrons. To allow the release of GFP during the infection, its coding sequence was  
148 flanked at both sides by synonymous sequences encoding the NIaPro cleavage site  
149 located between HAM1 and CP (LTIDVQ/A). First, eGFP (F64L, S65A, V163A)  
150 coding sequence was amplified by PCR with primers #3360/#3361, adding the coding  
151 sequence of NIaPro cleavage site in the reverse primer, by using P1P1b clone  
152 (Carbonell et al., 2012) as template. Then, the N-terminus of NIb and the whole HAM1  
153 coding sequences were amplified by PCR with primers #3160/#3358, adding the coding  
154 sequence of the NIaPro cleavage site in the reverse primer, by using pLX-UCBSVi as  
155 template. A subsequent overlapping PCR with primers #3160/#3361 was used to join  
156 the two above-mentioned PCR products into one single DNA segment. Finally, a  
157 BstBI/StuI fragment (the last 25 nt from NIb, the whole HAM1 and 1 nt from CP) from  
158 pLX-UCBSVi was replaced by the larger PCR product digested with BstBI.

159 To generate a 2xMyc-tagged version of HAM1 in UCSBV, pLX-UCBSVi was used as  
160 backbone to introduce the 2xMYC (GLINGEQKLISEEDLNGEQKLISEEDL) coding  
161 sequence just upstream the coding sequence that corresponds to the NIaPro cleavage  
162 site located between HAM1 and CP. First, the N-terminus of NIb and most of HAM1  
163 coding sequences were PCR amplified with primers #3160/#3162, adding the coding  
164 sequence of 1xMyc in the reverse primer, by using pLX-UCBSVi as template. Then, a  
165 second PCR with primers #3160/#3163, adding the coding sequence of another 1xMyc  
166 and the NIaPro cleavage site (LTIDVQ/) in the reverse primer, was carried out by using  
167 the first PCR product as template. Finally, a BstBI/StuI fragment (the last 25 nt from  
168 NIb, the whole HAM1 and 1 nt from CP) from pLX-UCBSVi was replaced by the  
169 second PCR product digested with BstBI/StuI to generate pLX-UCBSVi-2xMyc.

170 Mutagenesis of HAM1 in both pLX-UCBSVi and pLX-UCBSVi-HAM1-2xMyc  
171 backbones was done by using a previously described method (Ho et al., 1989). In brief,  
172 two PCR products having overlapping ends, which carry the desired mutation, were  
173 used as template of a subsequent PCR to join both PCR products in a larger DNA  
174 fragment. Then, a BstBI/StuI fragment (the last 25 nt from NIb, the whole HAM1 and 1  
175 nt from CP) in the corresponding backbone was replaced by the indicated PCR products  
176 digested with the same enzymes. A list of pLX-UCBSVi- and pLX-UCBSVi-HAM1-  
177 2xMyc-derivatives, as well as the name of primers used for the amplification of  
178 different inserts, are listed in Supplementary table S2.

179 The plasmid that expresses UCBSV-HAM1<sub>T1A/D3G</sub>-2xMyc, a double mutant that carries  
180 T1A and D3G mutations in HAM1, was generated by replacing the BstBI/StuI fragment  
181 in pLX-UCBSVi-HAM1-2xMyc with the RT-PCR product amplified with primers  
182 #3160/#3130 from RNA of a cassava plant originally infected with UCBSV-HAM1<sub>T1A</sub>-  
183 2xMyc after its digestion with the same restriction enzymes.

184 The plasmid pLX-UCBSVi-ΔHAM1, which has a full deletion of HAM1 cistron, was  
185 built by replacing the above-mentioned BstBI/StuI fragment in pLX-UCBSVi with a  
186 compatible end, short, double-stranded DNA fragment created by the annealing of  
187 oligonucleotides #3312/#3313.

188 Plasmids for transient expression of viral proteins in *N. benthamiana* leaves were built  
189 by the Gateway technology (Invitrogen) using pENTR1A as entry vector, and either  
190 pGWB702Ω (35S promoter, TMV 5'UTR, no tag, NOS terminator) or pGWB718 (35S  
191 promoter, 4xMyc tag for N-terminal fusion, NOS terminator) (Tanaka et al., 2011) as  
192 expression vectors. Briefly, cDNA fragments encoding NIa and NIb<sub>C</sub>-HAM1-CP<sub>N</sub> from  
193 UCBSV, CBSV and EuRV were amplified by PCR and directly introduced into  
194 pENTR1A previously digested with XmnI/EcoRV (name of primers and templates used  
195 for each PCR are indicated in Supplementary table S3). The correctness of pENTR1A  
196 derivatives was confirmed by digestion with restriction enzymes and Sanger sequencing  
197 by Macrogen Europe. Then, those cDNAs were moved from pENTR1A derivatives to  
198 either pGWB702Ω (NIa) or pGWB718 (NIb<sub>C</sub>-HAM1-CP<sub>N</sub>) by LR recombination.

199

200 **Alignment of primary amino acid sequences and 3D protein modeling.** The primary  
201 amino acid sequences of the following HAM1 proteins were downloaded from NCBI:  
202 human ITPA (NP\_258412.1), *E. coli* RdgB (NP\_417429.1), yeast HAM1  
203 (NP\_012603.1), arabidopsis HAM1-like protein (NP\_567410.1), and viral HAM1-like

204 proteins from CBSV (ACS71538.1), UCBSV (ASG92166.1) and EuRV  
205 (YP\_009310049.1). Protein sequences were aligned with Clustal Omega from EMBL-  
206 EBI (Madeira et al., 2019) with default parameters, and results were visualized/colored  
207 with Jalview version 2.11.1.4 (Waterhouse et al., 2009). The tridimensional structure of  
208 UCBSV HAM1 bound to ITP was modeled by homology using the SWISS-MODEL  
209 server (Waterhouse et al., 2018).

210

211 **Virus inoculation.** Inoculation of UCBSV full-length clones (wild type and  
212 derivatives) was carried out by biolistic with the Helios Gene Gun System (Bio-Rad) by  
213 following a previously described protocol (Salvador et al., 2008). Helium pressures of 7  
214 and 13 bar were used to inoculate *N. benthamiana* and cassava, respectively. Serial  
215 passages were done by manual inoculation of plants with sap extracts from infected  
216 plants as viral source. To do that, infected leaves were ground in a buffer containing 150  
217 mM NaCl, 2.5 mM DTT and 50 mM Tris-HCl pH 7.5 (2ml/mg) with an ice-cold mortar  
218 and pestle, and the sap was finger-rubbed onto two leaves of plants that had previously  
219 been dusted with Carborundum.

220

221 **Fluorescence imaging.** GFP fluorescence was observed with an epifluorescence  
222 stereomicroscope using excitation and barrier filters at 470/40 nm and 525/50 nm,  
223 respectively, and photographed with an Olympus DP70 digital camera.

224

225 **Transient expression by agro-infiltration.** Two young leaves of 1-month-old *N.*  
226 *benthamiana* plants were infiltrated with *Agrobacterium tumefaciens* strain C58C1  
227 carrying the indicated plasmids, as previously described (Valli et al., 2006). To boost  
228 protein expression, the potent silencing suppressor P14 from photos latent virus (Merai  
229 et al., 2005) was co-express along with the proteins of interest.

230

231 **Immunodetection of proteins by western blot.** The preparation of protein samples  
232 under denaturing conditions, the separation on SDS-PAGE and the electroblotting to  
233 nitrocellulose membranes was previously described (Gallo et al., 2018). UCBSV was  
234 detected using anti-CP (Ref. AS-1153, DSMZ) as primary antibody and horseradish  
235 peroxidase (HRP)-conjugated goat anti-rabbit IgG (Ref. 111-035-003, Jackson  
236 ImmunoResearch) as the secondary reagent. GFP and Myc-tag were detected using anti-  
237 GFP (Ref. 11814460001, Roche) and anti-Myc (either Ref. M20002, AbMART; or Ref.

238 05-724, Millipore) as primary antibodies, respectively, and HRP-conjugated sheep anti-  
239 mouse IgG (Ref. NA931, Amersham) as the secondary reagent. Immunostained proteins  
240 were visualized by enhanced chemiluminescence detection with Clarity ECL Western  
241 blotting substrate (Bio-Rad) in a ChemiDoc apparatus (Bio-Rad). Ponceau red was used  
242 to verify equivalent loading of total proteins in each sample.

243

244 **Reverse transcription followed by PCR.** Firstly, total RNA was isolated from *N.*  
245 *benthamiana* and cassava leaves by using the FavorPrep Plant Total RNA Purification  
246 Mini Kit (Ref. FAPRK 001, Favorgen Biotech) and Spectrum Plant Total RNA Kit  
247 (Ref. STRN50, Sigma), respectively. The RNA integrity was verified by electrophoresis  
248 in agarose gel. Secondly, cDNA was synthesized from 500 ng of total RNA with  
249 retrotranscriptase from Moloney murine leukemia virus (Ref. M0253, New England  
250 BioLabs) and random hexanucleotides as primers by following the manufacturer's  
251 instructions. Then, the cDNAs were used as template to amplify the region that encodes  
252 NI<sub>bC</sub>-HAM1-CP<sub>N</sub> with primers #3160/#3130 or the one that encodes a short fragment  
253 of CP with primers #3547/#3130. In the particular case of samples from cassava, which  
254 are prone to be contaminated with RT-PCR inhibitors such as polyphenols, RNA  
255 quality was checked by RT-PCR amplification of the UBQ10 housekeeping gene  
256 (Moreno et al., 2011) in order to validate the lack of amplification of UCBSV-derived  
257 fragments in samples from non-infected plants. Finally, when required, PCR products  
258 were Sanger sequenced by Macrogen Europe.

259

260 **Measurement of NTPs in plant leaves.** Free NTPs were extracted from young leaves  
261 of *N. benthamiana* and cassava by using a previously described method (Riondet et al.,  
262 2005). Extracts were immediately injected into a Vanquish UHPLC system equipped  
263 with a Q Exactive Focus Orbitrap spectrometry detector (Thermo Fisher Scientific).  
264 NTPs were separated by means of a Primesep SB column (3 μm, 4.6 x 150 mm)  
265 (SIELC Technologies) with a mobile phase formed by a mixture of (A) acetonitrile and  
266 water (5/95 v/v) with 30 mM of ammonium acetate (pH 4.5) and (B) acetonitrile and  
267 water (10/90 v/v) with 200 mM of ammonium acetate (pH 4.5) flowing at 1.0 ml/min  
268 with a gradient from 50-to-100% of A in 15 minutes. Injection was set to 5 μl and the  
269 column temperature to 25°C. Electrospray ionization was done at 4000V, setting the  
270 capillary temperature to 400°C. Desolvation was carried out with nitrogen with sheath  
271 gas and auxiliary gas flow rates of 70 and 20 (500°C), respectively. NTPs were detected



272 in MS/MS experiments (scan range from 50 to 550) based on the transition from the  
273 molecular protonated cation ( $[M+H]^+$ ) to the breakdown product consisting of the  
274 corresponding protonated nucleobase ( $[Nb+H]^+$ ) at collision energy of 25 eV.

275

## 276 **Results**

### 277 **UCBSV does not require HAM1 to infect *N. benthamiana*.**

278 With the aim of tracking the UCBSV infection *in planta*, an UCBSV full-length cDNA  
279 clone was manipulated to introduce the GFP coding sequence between N1b and CP  
280 cistrons (Figure 1A). The infection efficiency of UCBSV-eGFP was compared with that  
281 of the wild-type UCBSV in the model plant *N. benthamiana*. Plants inoculated with the  
282 wild-type virus (n=3) started to display clear symptoms of viral infection in upper non-  
283 inoculated leaves at 10 dpi, whereas those inoculated with UCBSV-eGFP (n=3) had a  
284 delay in symptom appearance of 2-to-3 days. At 15 dpi all inoculated plants showed  
285 equivalent symptoms in apical leaves, including strong leaf curling and vein clearing  
286 (Figure 1B); however, in line with the delay in symptom appearance, the height of  
287 plants inoculated with UCBSV-eGFP was in the middle of the untreated plants (tallest)  
288 and those infected with the wild-type UCBSV (shortest) (Figure 1B). As expected,  
289 upper non-inoculated leaves of plants infected with UCBSV-eGFP displayed GFP-  
290 derived fluorescence when observed under UV light (Figure 1B). In accordance with the  
291 other infection parameters, viral load in upper non-inoculated leaves, inferred from  
292 UCBSV CP immunodetection, was slightly higher in plants infected with the wild-type  
293 virus (Figure 1C). The immunodetection analysis also showed that GFP produced by  
294 UCBSV-eGFP was properly released from the viral polyprotein during the infection  
295 (Figure 1C).

296 After a plant-to-plant passage, unlike in plants initially inoculated with cDNA clones,  
297 we observed no differences among plants infected with wild-type and GFP-tagged  
298 viruses regarding the time of appearance and intensity of systemic symptoms. When  
299 upper non-inoculated leaves of plants infected with UCBSV-eGFP were observed under  
300 UV light at 20 dpi, curiously, fluorescence was not detected, suggesting that the GFP  
301 cistron had been deleted from the viral genome (data not shown). Indeed, a deeper  
302 analysis of viral populations from these plants confirmed this assumption, as DNA  
303 products amplified by RT-PCR with primers flanking the HAM1-GFP coding region  
304 were much smaller than those produced from plants originally infected by shooting  
305 (Figure 1D). Remarkably, direct Sanger sequencing of these products showed that not

306 only GFP-, but also HAM1-coding sequences, had been either totally or partially  
307 deleted from UCBSV-eGFP after the first passage (Figure 1D). This result support the  
308 idea that HAM1 is not required for the virus to infect *N. benthamiana*.

309

310 To confirm that HAM1 is unnecessary for UCBSV to infect the experimental host *N.*  
311 *benthamiana*, and rule out the possibility that a small fraction of the wild-type virus was  
312 complementing the deletion mutant, we built an infectious cDNA clone that carries a  
313 complete deletion of HAM1 cistron (Figure 2A). *N. benthamiana* plants inoculated with  
314 plasmids expressing either UCBSV or UCBSV- $\Delta$ HAM1 (n=3 per construct) started to  
315 display clear infection symptoms in upper non-inoculated leaves at the same time, and  
316 these symptoms were similar in intensity and type (Figure 2B). Estimation of viral load  
317 in these plants was carried out in samples from systemically infected leaves by RT-  
318 qPCR to detect small differences, if any. As observed in Figure 2C, accumulation of  
319 viral RNA did not show significant differences between both viruses. Together,  
320 experiments shown in Figure 1 and 2 demonstrate that HAM1 is not required to produce  
321 an UCBSV wild-type-like infection in *N. benthamiana*.

322

### 323 **UCBSV requires HAM1 pyrophosphatase activity to infect its natural host.**

324 Based on the above results, we hypothesized that the presence of HAM1 in UCBSV is a  
325 specific requirement for the virus to infect its natural host. To test this guess, we  
326 inoculated cassava and *N. benthamiana* plants in parallel with UCBSV and UCBSV-  
327  $\Delta$ HAM1 (n=3 per virus and plant species). As in the previous experiment, *N.*  
328 *benthamiana* plants displayed clear symptoms of UCBSV infection at 9-to-10 dpi in  
329 upper non-inoculated leaves independently of the presence/absence of HAM1 cistron in  
330 the viral genome (data not shown). Cassavas, in turn, developed typical UCBSV  
331 symptoms (yellow mottling along the major veins in leaves and dark brown streaks in  
332 stems) by 45-to-60 dpi in plants inoculated with the wild-type virus (Figure 2D). In  
333 contrast, plants inoculated with UCBSV- $\Delta$ HAM1, as those untreated, had normal leaf  
334 coloring and lacked streaks in stems (Figure 2D), even after 180 dpi (data not shown).  
335 The presence of UCBSV in these plants was tested by RT-PCR in samples collected at  
336 60 dpi from upper non-inoculated leaves. The result confirmed our visual observation:  
337 only plants inoculated with wild-type UCBSV accumulated viral RNA in upper non-  
338 inoculated tissues (Figure 2E).

339

340 Our results strongly suggest that UCBSV requires a pyrophosphatase activity to infect  
341 cassava. In order to test this hypothesis, and to rule out the possibility that the lack of  
342 infectivity of UCBSV- $\Delta$ HAM1 in cassava was rather due to an undesired side effect  
343 caused by the deletion of the whole HAM1 cistron from the viral genome, we aimed to  
344 introduce just a single point mutation in HAM1 to specifically disrupt its  
345 pyrophosphatase activity. Based on previous reports on the crystal structure of the  
346 human HAM1 (named ITPA) bound to ITP (Stenmark et al., 2007), we modeled with  
347 high confidence (QMEAN = -0.66) the tridimensional conformation of a UCBSV  
348 HAM1 dimer bound to this non-canonical nucleotide (Figure 3A). The K amino acid at  
349 position 38, which is located in the second  $\alpha$ -helix, is among the fully conserved amino  
350 acids in HAM1-like proteins from potyvirids and from organisms as diverse as  
351 *Escherichia coli*, baker's yeast, *Arabidopsis* and human (Supplementary Figure S1). In  
352 ITPA, this particular K (K19) is proposed to be part of the protein catalytic centre, as its  
353 side chain directly interacts with the triphosphate group of ITP (Stenmark et al., 2007)  
354 (Figure 3A). Moreover, in line with such relevance, a mutation of this K (K13) in  
355 RdgB, the HAM1-like protein from *E. coli*, abolishes its capacity to hydrolyze ITP *in*  
356 *vitro* (Savchenko et al., 2007). Based on these data, we build an UCBSV cDNA clone  
357 that carries the mutation K38A in HAM1 (Figure 3B). The wild-type and mutant  
358 versions of UCBSV were inoculated in *N. benthamiana* and cassava in parallel (n=3 per  
359 virus and plant species). As expected, there were no differences in *N. benthamiana*  
360 plants inoculated with each of these viruses in infectivity, time of appearance and  
361 intensity of symptoms in upper non-inoculated leaves (Figure 3C), as well as in viral  
362 accumulation measured by RT-qPCR in samples from these tissues (Figure 3D).  
363 Conversely, only the three cassava plants inoculated with the wild-type virus displayed  
364 symptoms of viral infection in upper non-inoculated leaves at 60 dpi (Figure 3E).  
365 Further analysis by RT-PCR confirmed that the wild-type UCBSV, but not the mutant  
366 variant that carries the K38A mutation in HAM1, was able to infect cassavas (Figure  
367 3F).

368 Together, these results indicate that an active pyrophosphatase contributes to UCBSV  
369 infection, and the requirement of this activity depends on the particular host.

370

### 371 **Differential accumulation of NTPs in *M. esculenta* versus *N. benthamiana*.**

372 Our observation that pyrophosphatase activity is only required for UCBSV infection in  
373 cassava prompted us to investigate the accumulation of canonical and non-canonical

374 nucleotides in *M. esculenta* and *N. benthamiana* plants. To do that, NTPs were extracted  
375 from equivalent amount of tissue powder from both UCBSV hosts (n=12 per plant  
376 species) and the relative concentrations of ATP, CTP, GTP, UTP, ITP and XTP were  
377 estimated by high performance liquid chromatography coupled with tandem mass  
378 spectrometry. Whereas the concentration (measured as the area under the curve)  
379 corresponding to CTP and ATP were equivalent in both plants, showing no significant  
380 differences, that of XTP, ITP, GTP and UTP were significantly higher in cassava  
381 relative to *N. benthamiana* (Figure 4A). This difference was particularly relevant in the  
382 case of the non-canonical nucleotides XTP (4.5 folds) and ITP (3.6 folds) (Figure 4B).  
383 Importantly, an independent repetition of this experiment showed equivalent differences  
384 when comparing the population of NTPs in leaves of these two plant species. Therefore,  
385 we can conclude that *M. esculenta*, the natural host of UCBSV, accumulates much  
386 higher levels of XTP and ITP in leaves than the *N. benthamiana* counterpart.

387

#### 388 **Suboptimal cleavage at Nib/HAM1 junction during UCBSV infection.**

389 When the presence of HAM1 cistron in the genome of UCBSV (named CBSV at that  
390 time) was reported for the first time, authors proposed that Nib and HAM1 might  
391 accumulate as two independent mature factors in infected cells due to the presence of a  
392 putative target for the viral-derived protease NIaPro (Mbanzibwa et al., 2009). A  
393 canonical NIaPro cleavage site is formed by 9 moderately conserved amino acids, and  
394 cleavage occurs between residues 6 and 7 (P1 and P1', Figure 5A). Amino acid primary  
395 sequence analysis shows that positions P4, P1 and P1' have high degree of  
396 conservation. For P1', for instance, either A, S or G residues were observed in 92% of  
397 the cases (n = 343 from 49 viral genomes × 7 cleavage sites (Adams et al., 2005).  
398 Curiously, a T residue occupies this position in the cleavage site located at the  
399 Nib/HAM1 junction of UCBSV (Figure 5A), which is not a common amino acid at P1'  
400 with a representation of 2%. In fact, a seminal study about the NIaPro-mediated  
401 cleavage at the Nib/CP junction of tobacco etch virus, another potyvirus, showed that S  
402 x T mutation at P1' strongly reduced cleavage efficiency in an *in vitro* system (see  
403 Figure 4D in (Dougherty et al., 1988).

404 The above-mentioned antecedents prompted us to investigate whether the proposed  
405 cleavage site located between Nib and HAM1 is efficiently processed during UCBSV  
406 infection. To do that we built an infectious cDNA clone in which HAM1 was tagged  
407 with two copies of the Myc epitope (UCBSV-HAM1-2xMyc, Figure 5B) for the easy

408 detection of HAM1 in extracts of infected tissues. This clone, and the clone that  
409 expresses the wild-type UCBSV as control, were inoculated in *N. benthamiana* plants  
410 (n=3 per virus). No differences among inoculated plants were observed in term of viral  
411 symptoms (Figure 5C) and accumulation as estimated by western blot against UCBSV  
412 CP (Figure 5D). This result indicated that the tag does not have a noticeable negative  
413 impact on viral fitness in *N. benthamiana*. Immunodetection with Myc antibody  
414 revealed the presence of two defined protein species in samples infected with UCBSV-  
415 2xMYC. The one with less electrophoretic mobility had the expected size for the Myc-  
416 tagged Nib-HAM1 fusion product (86.3 kDa), whereas the smaller species had the  
417 expected size for the sole Myc-tagged HAM1 (28.2 kDa) (Figure 5D). The ratio  
418 between larger and smaller species was estimated in 1.5 based on the densitometric  
419 analysis of chemiluminescence signals.

420 Our results, along with previous antecedents (see above), suggested that T at position  
421 P1' causes an inefficient NlaPro-mediated processing at the cleavage site located in the  
422 Nib/HAM1 junction. To test this idea, we introduced mutations in the UCBSV cDNA  
423 clone to express two types of P1' mutants: (i) T1A and T1S, as A and S are among the  
424 most frequent residues at this position, and (ii) TxP, as P is not present at the P1'  
425 position in any NlaPro cleavage sites (Adams et al., 2005). When mutated and wild-  
426 type versions of UCBSV-2xMYC were inoculated in *N. benthamiana* (n=2 per virus),  
427 all of them produced indistinguishable infections, with comparable symptoms  
428 (Supplementary Figure 2) and virus accumulation in upper non-inoculated leaves as  
429 observed by immunodetection of UCBSV CP (Figure 5E). As anticipated from  
430 conservation of amino acids present at the P1' position, the T1A and T1S mutants  
431 accumulated only the protein species that corresponds to free HAM1, while T1P mutant  
432 only produced the Nib-HAM1 complex. Altogether, these results indicate that the  
433 NlaPro-mediated separation of Nib and HAM1 is inherently inefficient in UCBSV,  
434 which is due to the presence of a T residue at the P1' position of the cleavage site.

435

#### 436 **Relevance of the inefficient cleavage at Nib/HAM1 junction in cassava.**

437 To estimate the relevance of the poor separation of Nib from HAM1 in the UCBSV  
438 natural host, we inoculated cassava plants with the Myc-tagged wild-type virus as well  
439 as the T1A and T1P variants (n=3 per virus). Clear symptoms of infection appeared at  
440 60 dpi in the upper leaves of all inoculated plants independently of the infecting virus  
441 (Figure 6A). At that time, RT-PCR confirmed that upper non-inoculated leaves from all

442 inoculated plants were successfully infected with the Myc-tagged viruses (Figure 6B).  
443 Moreover, Sanger sequencing analysis of these RT-PCR products indicated that the  
444 introduced mutations were maintained after two months (Figure 6C). At 120 dpi, we  
445 divided plants infected with each virus in two groups, such as one plant was kept  
446 growing (plant 1), whereas the remaining two plants were propagated through stem  
447 cuttings (plant 2 and plant 3). At 180 dpi, samples were taken from the upper leaves of  
448 all plants and the identity of infecting viruses was determined. Remarkably, whereas the  
449 NIB-HAM1 junction from both wild-type and the T1P variants remained unchanged in  
450 all the analyzed plants (data not shown), that of the T1A variant evolved to introduce  
451 mutations (Figure 6C and Supplementary Figure S3). In the case of plant 1, a second  
452 mutation appeared at the P3' position, so that the original D amino acid was replaced by  
453 G (D3G) to give rise to a T1A/D3G double mutant (Figure 6C). Cuttings made from  
454 plant 2 also accumulated a viral variant carrying the second mutation G3D, reinforcing  
455 the idea that the T1A single mutant evolves to T1A/D3G when adapting to cassava  
456 (Supplementary Figure S3). Finally, cuttings made from plant 3 showed accumulation  
457 of a variant that encodes the wild-type cleavage site, so that the T1A mutation reverted  
458 to T (Supplementary Figure S3).

459 The observed reversion in cuttings from plant 3 strongly suggested that the virus  
460 requires the inefficient processing of the cleavage site located at the NIB-HAM1  
461 junction for a successful infection. If that were the case, then one would expect that the  
462 T1A/D3G double mutant mimics this phenotype. To test this idea, we built the double  
463 mutant T1A/D3G by directed mutagenesis of the UCBSV-HAM1-2xMyc clone, and  
464 this plasmid was used to inoculate *N. benthamiana* plants (n=4) for easy detection of  
465 processing products by western blot. Both UCBSV-HAM1-2xMyc and UCBSV-  
466 HAM1<sub>T1A</sub>-2xMyc variants were used as control (n=2 per variant). The T1A/D3G  
467 double mutant behaved as controls in term of infection timing and visible symptoms  
468 (data not shown), as well as viral accumulation in upper non-inoculated leaves as  
469 estimated by immunodetection of UCBSV CP (Figure 6D). Detection of Myc-tagged  
470 proteins in samples from systemically infected tissue showed that the T1A/D3G double  
471 mutant, as in the case of the wild-type virus, and unlike the T1A variant, accumulated  
472 two different protein species: NIB-HAM1 and free HAM1 (Figure 6D). Therefore, our  
473 results indicate that, at least for a relevant fraction of the total NIB and HAM1 produced  
474 during UCBSV infection, (i) these two proteins stay covalently bound, and (ii) the NIB-  
475 HAM1 partnership is indeed essential when UCBSV infects its natural host. In addition,

476 our viral evolution experiment highlights the importance of the usually underestimated  
477 amino acids located at P3' position of NIaPro cleavage sites for the actual NIaPro  
478 processing.

479

480 **The expression of a joint NIB-HAM1 product is a common feature of potyvirids**  
481 **encoding HAM1.**

482 CBSV and EuRV are also potyvirids encoding HAM1 in their genomes, and this cistron  
483 is located, as in the case of UCBSV, just downstream of NIB. Importantly, the  
484 previously proposed NIaPro cleavage site at the NIB/HAM1 junction in both viruses  
485 (Mbanzibwa et al., 2009) does not fit the conventional conservation rules. CBSV has a  
486 V at P1', which is not a common residue at this position (Figure 5A) (Adams et al.,  
487 2005). In the case of EuRV, P1 is occupied by R, which is a strongly underrepresented  
488 amino acid at this position (Figure 5A) (Adams et al., 2005). Therefore, we  
489 hypothesized that HAM1 also remains bound to CBSV and EuRV NIBs. To test this  
490 idea, and due to the lack of infectious cDNA clones for these two viruses, we transiently  
491 expressed 4xMyc c-terminal tagged versions of NIB-HAM1-CP either with or without  
492 the presence of their cognate NIa (VPg-NIaPro) proteinases (Figure 7A). We did the  
493 same with the equivalent fragments of UCBSV as control for comparison. As expected,  
494 the expression of UCBSV fragments mimicked the results that we got with the full-  
495 length UCBSV-2xMYC virus, so that NIB-HAM1-CP was processed only in the  
496 presence of NIa, and it happened at the cleavage site located at the HAM1/CP junction  
497 and, with much lower efficiency, at the site placed at the NIB/HAM1 junction (Figure  
498 7B). Remarkably, CBSV behaved just like UCBSV, as the main product, by far, was the  
499 one produced after cleavage at the HAM1/CP junction, with just a residual  
500 accumulation of the small fragment corresponding to the processing at the NIB/HAM1  
501 junction (Figure 7B). Finally, for EuRV we only detected the product that corresponds  
502 to the NIaPro-mediated processing of the cleavage site located between HAM1 and CP  
503 (Figure 7B). Altogether, we conclude that most of the NIB and HAM1 might also be  
504 covalently bound during CBSV and EuRV infections.

505

506 **Discussion**

507 RNA viruses are widespread in nature, where they display a great diversity of particle  
508 structures, genome arrangements and expressed proteins (Dolja and Koonin, 2018).  
509 Despite these differences, they are all replicated by viral-encoded RdRPs sharing, at

510 least in all cases reported so far, a highly conserved core architecture folded into three  
511 subdomains (thumb, palm, and fingers) resembling a cupped right hand (Venkataraman  
512 et al., 2018). In some cases, other key protein domains implicated in viral replication,  
513 and/or transcription, are acquired by basic RdRP cores. The flaviviral replicase (NS5),  
514 for instance, possesses a capping enzyme domain required to synthesize the 5'-cap  
515 structure of genomic RNA (Lu and Gong, 2017, Brand et al., 2017). The potexviral  
516 replicase, in turn, not only has a capping enzyme domain, but also a helicase (Park et  
517 al., 2013). Remarkably, the covalent association between a viral RdRP and a HAM1-  
518 like protein had not been described so far. Data presented in this study indicate that (i)  
519 particular potyvirus replicases are covalently bound to, and work in association with, a  
520 HAM1-like pyrophosphatase, and (ii) the requirement of this partnership is host  
521 specific, which might be due to the peculiar accumulation of XTP/ITP in some hosts.  
522 Regarding the precise role of viral HAM1 enzymes during the infection, the simple fact  
523 that a high fraction of this protein stays covalently attached to the viral replicase  
524 strongly suggests that HAM1 participates in replication. As UCBSV- and CBSV-  
525 derived HAM1s are pyrophosphatases with preference for non-canonical nucleotides  
526 (Tomlinson et al., 2019), it is logical to hypothesize that HAM1 hydrolyses ITP/XTP in  
527 order to prevent their incorporation into the viral genome, which would otherwise  
528 cause inhibition of RNA synthesis and/or further genome mutations. In other words, it  
529 seems quite likely that ITP/XTP behave as natural antiviral molecules, similarly to  
530 artificial nucleoside- and nucleotide-like analogues used against plus-stranded RNA  
531 viruses in animals (Deval et al., 2014). Intriguingly, our experiments with UCBSV (data  
532 not shown), as well as previous results with CBSV (Tomlinson et al., 2019), showed  
533 that the absence of HAM1 does not increase the complexity of UCBSV and CBSV  
534 mutant swarms in infected *N. benthamiana* plants. The incapacity of pyrophosphatase-  
535 defective UCBSV variants to infect cassava (Figure 2 and 3) precluded us to test  
536 whether the absence of this activity increases the variability of UCBSV genome  
537 sequence in its natural host, where HAM1 is strictly required.  
538 Theoretically, the concentration of ITP/XTP in the pool of free nucleotides inside cells  
539 are tightly maintained at low levels by ITPases to avoid their deleterious effects over  
540 DNA and RNA molecules (Simone et al., 2013). Therefore, results showing that  
541 cassava, and probably other euphorbiaceous, accumulates high amounts of ITP/XTP  
542 (Figure 4) question this rule. To conciliate our result in cassava with that broadly  
543 accepted idea, we hypothesize that some plants accumulate unexpectedly high



544 concentration of ITP/XTP in certain subcellular compartments, whereas in those  
545 locations where they have damaging consequences, such as in the nucleus, ITP/XTP are  
546 kept at much lower concentration. The recent suggestion that euphorbiaceous HAM1-  
547 like proteins might harbour a nuclear localization signal (James et al., 2021) fits pretty  
548 well with this assumption. Therefore, it is possible that viruses infecting plants from the  
549 *Euphorbiacea* family (e.g. UCBSV, CBSV, EuRV and CsTLV) have to face high levels  
550 of ITP/XTP in the cytoplasm, where they replicate, thus explaining the incorporation of  
551 a HAM1 enzyme as an active module of the viral replicase. This possibility also fits  
552 well with the expression of some free HAM1 during the infection (Figure 5, 6 and 7), so  
553 that it might also help to get rid of ITP/XTP in all those cellular environments where the  
554 virus is replicating.

555 All in all, our findings inform about a novel and interesting case of virus/host  
556 coevolution, highlighting (i) the striking peculiarity of cassava plants, and presumably  
557 other euphorbiaceous, of accumulating high levels of ITP/XTP into cells, and (ii) the  
558 flexibility of RNA viruses to incorporate additional factors when required. Whether this  
559 peculiar feature of cassava regarding the high concentration of non-canonical  
560 nucleotides evolved as a *bona fide* strategy to prevent multiplication of pathogens, and  
561 how this plant copes with the harmful effect of ITP/XTP, are indeed exciting questions  
562 deserving special attention in future studies.

563

#### 564 **Acknowledgments.**

565 We would like to thank Tsuyoshi Nakagawa, Daniel Silhavy and Gary Foster, for  
566 providing Gateway expression vectors, pBIN61-P14 and pYES2-CBSV-F2,  
567 respectively. We are also grateful to the Mass Spectrometry Facility (Nucleus, USAL)  
568 for its kind help. This work was funded by BIO2015-73900-JIN (AEI-FEDER),  
569 PID2019-110979RB-I00/ AEI / 10.13039/501100011033, RYC2018-025523-I and  
570 202020E001 to A.A.V, BIO2016-80572-R (AEI-FEDER) and PID2019-109380RBI00/  
571 AEI /301 10.13039/501100011033 to J.A.G, and Funding Program for Research Groups  
572 (M.C2 from USAL) to D.G.G.

573

#### 574 **Author contribution**

575 Conceptualization, A.A.V, J.A.G; Investigation, A.A.V, R.G.L., M.R., F.J.M, D.G.G.,  
576 B.G.; I.G., A.G.P. and I.M.; Writing – Original Draft, A.A.V.; Writing – Review &

577 Editing, A.A.V, J.A.G.; Funding Acquisition, A.A.V, J.A.G., D.G.G.; Resources, F.P.;  
578 Supervision, A.A.V.

579

## 580 Declaration of interests

581 The authors declare no competing interests.

582

## 583 References

584

- 585 ADAMS, M. J., ANTONIW, J. F. & BEAUDOIN, F. 2005. Overview and analysis of  
586 the polyprotein cleavage sites in the family Potyviridae. *Mol Plant Pathol*, 6,  
587 471-87.
- 588 ALLISON, R., JOHNSTON, R. E. & DOUGHERTY, W. G. 1986. The nucleotide  
589 sequence of the coding region of tobacco etch virus genomic RNA: evidence for  
590 the synthesis of a single polyprotein. *Virology*, 154, 9-20.
- 591 BRAND, C., BISAILLON, M. & GEISS, B. J. 2017. Organization of the Flavivirus  
592 RNA replicase complex. *Wiley Interdiscip Rev RNA*, 8.
- 593 CARBONELL, A., DUJOVNY, G., GARCIA, J. A. & VALLI, A. 2012. The Cucumber  
594 vein yellowing virus silencing suppressor P1b can functionally replace HCPro in  
595 Plum pox virus infection in a host-specific manner. *Mol Plant Microbe Interact*,  
596 25, 151-64.
- 597 CARRINGTON, J. C. & DOUGHERTY, W. G. 1987a. Processing of the tobacco etch  
598 virus 49K protease requires autoproteolysis. *Virology*, 160, 355-62.
- 599 CARRINGTON, J. C. & DOUGHERTY, W. G. 1987b. Small nuclear inclusion protein  
600 encoded by a plant potyvirus genome is a protease. *J Virol*, 61, 2540-8.
- 601 CHUNG, J. H., BACK, J. H., PARK, Y. I. & HAN, Y. S. 2001. Biochemical  
602 characterization of a novel hypoxanthine/xanthine dNTP pyrophosphatase from  
603 *Methanococcus jannaschii*. *Nucleic Acids Res*, 29, 3099-107.
- 604 CHUNG, J. H., PARK, H. Y., LEE, J. H. & JANG, Y. 2002. Identification of the dITP-  
605 and XTP-hydrolyzing protein from *Escherichia coli*. *J Biochem Mol Biol*, 35,  
606 403-8.
- 607 DEVAL, J., SYMONS, J. A. & BEIGELMAN, L. 2014. Inhibition of viral RNA  
608 polymerases by nucleoside and nucleotide analogs: therapeutic applications  
609 against positive-strand RNA viruses beyond hepatitis C virus. *Curr Opin Virol*,  
610 9, 1-7.
- 611 DOLJA, V. V. & KOONIN, E. V. 2018. Metagenomics reshapes the concepts of RNA  
612 virus evolution by revealing extensive horizontal virus transfer. *Virus Res*, 244,  
613 36-52.
- 614 DOMBROVSKY, A., REINGOLD, V. & ANTIGNUS, Y. 2014. Ipomovirus--an  
615 atypical genus in the family Potyviridae transmitted by whiteflies. *Pest Manag*  
616 *Sci*, 70, 1553-67.
- 617 DOUGHERTY, W. G., CARRINGTON, J. C., CARY, S. M. & PARKS, T. D. 1988.  
618 Biochemical and mutational analysis of a plant virus polyprotein cleavage site.  
619 *EMBO J*, 7, 1281-7.
- 620 GALLO, A., VALLI, A., CALVO, M. & GARCIA, J. A. 2018. A Functional Link  
621 between RNA Replication and Virion Assembly in the Potyvirus Plum Pox  
622 Virus. *J Virol*, 92.

- 623 HILLOCKS, R. J. & MARUTHI, M. N. 2015. *Post-harvest impact of cassava brown*  
624 *streak disease in four countries in eastern Africa*, Practical Action Publishing.
- 625 HO, S. N., HUNT, H. D., HORTON, R. M., PULLEN, J. K. & PEASE, L. R. 1989.  
626 Site-directed mutagenesis by overlap extension using the polymerase chain  
627 reaction. *Gene*, 77, 51-9.
- 628 HONG, Y. & HUNT, A. G. 1996. RNA polymerase activity catalyzed by a potyvirus-  
629 encoded RNA-dependent RNA polymerase. *Virology*, 226, 146-51.
- 630 HWANG, K. Y., CHUNG, J. H., KIM, S. H., HAN, Y. S. & CHO, Y. 1999. Structure-  
631 based identification of a novel NTPase from *Methanococcus jannaschii*. *Nat*  
632 *Struct Biol*, 6, 691-6.
- 633 JAMES, A. M., SEAL, S. E., BAILEY, A. M. & FOSTER, G. D. 2021. Viral inosine  
634 triphosphatase: A mysterious enzyme with typical activity, but an atypical  
635 function. *Mol Plant Pathol*, 22, 382-389.
- 636 JIMÉNEZ POLO, J., LEIVA, A. M. & CUELLAR, W. J. 2018. Identification of a  
637 torradovirus-encoded protein that complements the systemic movement of a  
638 potyvirus lacking the TGB3 gene. *International Congress of Plant Pathology*  
639 *(ICPP) 2018: Plant Health in A Global Economy, Boston*.
- 640 KNIERIM, D., MENZEL, W. & WINTER, S. 2017. Analysis of the complete genome  
641 sequence of euphorbia ringspot virus, an atypical member of the genus  
642 Potyvirus. *Arch Virol*, 162, 291-293.
- 643 LIN, S., MCLENNAN, A. G., YING, K., WANG, Z., GU, S., JIN, H., WU, C., LIU,  
644 W., YUAN, Y., TANG, R., XIE, Y. & MAO, Y. 2001. Cloning, expression, and  
645 characterization of a human inosine triphosphate pyrophosphatase encoded by  
646 the itpa gene. *J Biol Chem*, 276, 18695-701.
- 647 LOPEZ-MOYA, J. J. & GARCIA, J. A. 2000. Construction of a stable and highly  
648 infectious intron-containing cDNA clone of plum pox potyvirus and its use to  
649 infect plants by particle bombardment. *Virus Res*, 68, 99-107.
- 650 LU, G. & GONG, P. 2017. A structural view of the RNA-dependent RNA polymerases  
651 from the Flavivirus genus. *Virus Res*, 234, 34-43.
- 652 MADEIRA, F., PARK, Y. M., LEE, J., BUSO, N., GUR, T., MADHUSOODANAN,  
653 N., BASUTKAR, P., TIVEY, A. R. N., POTTER, S. C., FINN, R. D. & LOPEZ,  
654 R. 2019. The EMBL-EBI search and sequence analysis tools APIs in 2019.  
655 *Nucleic Acids Res*, 47, W636-W641.
- 656 MBANZIBWA, D. R., TIAN, Y., MUKASA, S. B. & VALKONEN, J. P. 2009.  
657 Cassava brown streak virus (Potyviridae) encodes a putative Maf/HAM1  
658 pyrophosphatase implicated in reduction of mutations and a P1 proteinase that  
659 suppresses RNA silencing but contains no HC-Pro. *J Virol*, 83, 6934-40.
- 660 MERAI, Z., KERENYI, Z., MOLNAR, A., BARTA, E., VALOCZI, A., BISZTRAY,  
661 G., HAVELDA, Z., BURGYN, J. & SILHAVY, D. 2005. Aureusvirus P14 is  
662 an efficient RNA silencing suppressor that binds double-stranded RNAs without  
663 size specificity. *J Virol*, 79, 7217-26.
- 664 MORENO, I., GRUISSEM, W. & VANDERSCHUREN, H. 2011. Reference genes for  
665 reliable potyvirus quantitation in cassava and analysis of Cassava brown streak  
666 virus load in host varieties. *J Virol Methods*, 177, 49-54.
- 667 PARK, M. R., SEO, J. K. & KIM, K. H. 2013. Viral and nonviral elements in  
668 potyvirus replication and movement and in antiviral responses. *Adv Virus Res*,  
669 87, 75-112.
- 670 PASIN, F., BEDOYA, L. C., BERNABE-ORTS, J. M., GALLO, A., SIMON-MATEO,  
671 C., ORZAEZ, D. & GARCIA, J. A. 2017. Multiple T-DNA Delivery to Plants

- 672 Using Novel Mini Binary Vectors with Compatible Replication Origins. *ACS*  
673 *Synthetic Biology*, 6, 1962-1968.
- 674 PATIL, B. L., LEGG, J. P., KANJU, E. & FAUQUET, C. M. 2015. Cassava brown  
675 streak disease: a threat to food security in Africa. *J Gen Virol*, 96, 956-68.
- 676 PENNISI, E. 2010. Armed and dangerous. *Science*, 327, 804-5.
- 677 REVERS, F. & GARCÍA, J. A. 2015. Molecular biology of potyviruses. *Advances in*  
678 *Virus Research*, 92, 101-99.
- 679 RIONDET, C., MOREL, S. & ALCARAZ, G. 2005. Determination of total  
680 ribonucleotide pool in plant materials by high-pH anion-exchange high-  
681 performance liquid chromatography following extraction with potassium  
682 hydroxide. *J Chromatogr A*, 1077, 120-7.
- 683 SALVADOR, B., DELGADILLO, M. O., SAENZ, P., GARCIA, J. A. & SIMON-  
684 MATEO, C. 2008. Identification of Plum pox virus pathogenicity determinants  
685 in herbaceous and woody hosts. *Mol Plant Microbe Interact*, 21, 20-9.
- 686 SAVCHENKO, A., PROUDFOOT, M., SKARINA, T., SINGER, A., LITVINOVA, O.,  
687 SANISHVILI, R., BROWN, G., CHIRGADZE, N. & YAKUNIN, A. F. 2007.  
688 Molecular basis of the antimutagenic activity of the house-cleaning inosine  
689 triphosphate pyrophosphatase RdgB from Escherichia coli. *J Mol Biol*, 374,  
690 1091-103.
- 691 SCHECHTER, I. & BERGER, A. 1967. On the size of the active site in proteases. I.  
692 Papain. *Biochem Biophys Res Commun*, 27, 157-62.
- 693 SIMONE, P. D., PAVLOV, Y. I. & BORGSTAHL, G. E. 2013. ITPA (inosine  
694 triphosphate pyrophosphatase): from surveillance of nucleotide pools to human  
695 disease and pharmacogenetics. *Mutat Res*, 753, 131-46.
- 696 STENMARK, P., KURSULA, P., FLODIN, S., GRASLUND, S., LANDRY, R.,  
697 NORDLUND, P. & SCHULER, H. 2007. Crystal structure of human inosine  
698 triphosphatase. Substrate binding and implication of the inosine triphosphatase  
699 deficiency mutation P32T. *J Biol Chem*, 282, 3182-7.
- 700 TANAKA, Y., NAKAMURA, S., KAWAMUKAI, M., KOIZUMI, N. &  
701 NAKAGAWA, T. 2011. Development of a series of gateway binary vectors  
702 possessing a tunicamycin resistance gene as a marker for the transformation of  
703 Arabidopsis thaliana. *Biosci Biotechnol Biochem*, 75, 804-7.
- 704 TOMLINSON, K. R., BAILEY, A. M., ALICAI, T., SEAL, S. & FOSTER, G. D. 2018.  
705 Cassava brown streak disease: historical timeline, current knowledge and future  
706 prospects. *Mol Plant Pathol*, 19, 1282-1294.
- 707 TOMLINSON, K. R., PABLO-RODRIGUEZ, J. L., BUNAWAN, H., NANYITI, S.,  
708 GREEN, P., MILLER, J., ALICAI, T., SEAL, S. E., BAILEY, A. M. &  
709 FOSTER, G. D. 2019. Cassava brown streak virus Ham1 protein hydrolyses  
710 mutagenic nucleotides and is a necrosis determinant. *Mol Plant Pathol*, 20,  
711 1080-1092.
- 712 VALLI, A., GARCÍA, J. A. & LÓPEZ-MOYA, J. J. 2021. Potyviruses (Potyviridae).  
713 In: BAMFORD, D. H. & ZUCKERMAN, M. (eds.) *Encyclopedia of Virology*  
714 (*Fourth Edition*). Oxford: Academic Press.
- 715 VALLI, A., LOPEZ-MOYA, J. J. & GARCIA, J. A. 2007. Recombination and gene  
716 duplication in the evolutionary diversification of P1 proteins in the family  
717 Potyviridae. *J Gen Virol*, 88, 1016-28.
- 718 VALLI, A., MARTIN-HERNANDEZ, A. M., LOPEZ-MOYA, J. J. & GARCIA, J. A.  
719 2006. RNA silencing suppression by a second copy of the P1 serine protease of  
720 Cucumber vein yellowing ipomovirus, a member of the family Potyviridae that  
721 lacks the cysteine protease HCPro. *J Virol*, 80, 10055-63.

722 VENKATARAMAN, S., PRASAD, B. & SELVARAJAN, R. 2018. RNA Dependent  
723 RNA Polymerases: Insights from Structure, Function and Evolution. *Viruses*,  
724 10.  
725 WATERHOUSE, A., BERTONI, M., BIENERT, S., STUDER, G., TAURIELLO, G.,  
726 GUMIENNY, R., HEER, F. T., DE BEER, T. A. P., REMPFER, C., BORDOLI,  
727 L., LEPORE, R. & SCHWEDE, T. 2018. SWISS-MODEL: homology  
728 modelling of protein structures and complexes. *Nucleic Acids Res*, 46, W296-  
729 W303.  
730 WATERHOUSE, A. M., PROCTER, J. B., MARTIN, D. M., CLAMP, M. &  
731 BARTON, G. J. 2009. Jalview Version 2--a multiple sequence alignment editor  
732 and analysis workbench. *Bioinformatics*, 25, 1189-91.  
733 WINTER, S., KOERBLER, M., STEIN, B., PIETRUSZKA, A., PAAPE, M. &  
734 BUTGEREITT, A. 2010. Analysis of cassava brown streak viruses reveals the  
735 presence of distinct virus species causing cassava brown streak disease in East  
736 Africa. *J Gen Virol*, 91, 1365-72.  
737 YANG, X., LI, Y. & WANG, A. 2021. Research advances in potyviruses: From the  
738 laboratory bench to the field. *Annual Review of Phytopathology*, 59, *In Press*.  
739

#### 740 **Figure legends**

741 **Figure 1. GFP-tagged UCBSV loses HAM1 and GFP coding sequences after one**  
742 **passage in *N. benthamiana*.** (A) Schematic representation of viral constructs based on  
743 the pLX-UCBSV (Pasin et al., 2017) used in this experiment. Boxes represent mature  
744 viral factors as they are encoded in the viral genome. The presence of an intron in the  
745 P3 coding sequence is also indicated. p35S: 35S promoter from cauliflower mosaic  
746 virus; tNOS: terminator from the NOS gene of *Agrobacterium tumefaciens*. (B)  
747 Representative pictures taken at 15 days post-inoculation of infected and non-treated *N.*  
748 *benthamiana* plants under UV radiation and visible light (white bar = 1 cm; black bar =  
749 4 cm). (C) Detection of GFP and UCBSV CP by immunoblot analysis in protein  
750 samples from upper non-inoculated leaves of *N. benthamiana* plants infected with the  
751 indicated viruses. Blot stained with *Ponceau* red showing the large subunit of the  
752 ribulose-1,5-bisphosphate carboxylase-oxygenase is included as a loading control (D)  
753 Agarose gel electrophoresis analysis of a viral genomic fragment amplified by RT-PCR  
754 from plants infected with UCBSV-GFP after one passage. The upper part shows a  
755 schematic representation of the amplified fragment. Black arrows represent primers  
756 used for amplification. Sizes of expected PCR products are indicated. Amino acids  
757 around the NIaPro cleavage sites are depicted at the bottom.

758

759 **Figure 2. Virus-derived HAM1 is required for the successful infection of UCBSV**  
760 **in cassava plants, but not in *N. benthamiana*.** (A) Schematic representation of the

761 NIB-to-CP genomic segment of viruses used in these experiments. Amino acids around  
762 the NIaPro cleavage sites are depicted. (B) Representative pictures of infected and non-  
763 treated *N. benthamiana* plants taken at 12 days post-inoculation. White bar = 4 cm. (C)  
764 RT-qPCR measuring the accumulation of viral RNA in upper non-inoculated leaves of  
765 *N. benthamiana* plants infected with the indicated viruses. Each bar represents the  
766 average of three plants (error bar = 1 standard deviation). For normalization, the  
767 average of wild type UCBSV is equal to 1. (D) Representative pictures of upper non-  
768 inoculated leaves, at 60 days post-inoculation, of cassava plants inoculated with the  
769 indicated viruses. White bar = 4 cm. Black arrows indicates the presence of brown  
770 streaks in the stem of an infected plant. (E) Analysis by agarose gel electrophoresis of a  
771 fragment of the UCBSV genome (V) and of a plant housekeeping gene (H) amplified by  
772 RT-PCR. RNA samples from upper non-inoculated leaves of 3 independent cassava  
773 plants inoculated with the indicated viruses were used as template.

774

775 **Figure 3. The pyrophosphatase activity of UCBSV HAM1 is required for the**  
776 **successful infection of cassava plants.** (A) Model of the ITP-bound UCBSV HAM1  
777 tridimensional structure. Interaction between K38 and ITP is highlighted at the left. (B)  
778 Schematic representation of the NIB-to-CP genomic segment of viruses used in these  
779 experiments. Amino acids around the NIaPro cleavage sites are depicted. The presence  
780 of the K38A mutation is indicated with a red line. (C) Representative pictures of  
781 infected and non-treated *N. benthamiana* plants taken at 11 days post-inoculation.  
782 White bar = 4 cm. (D) RT-qPCR measuring the accumulation of viral RNA in upper  
783 non-inoculated leaves of *N. benthamiana* plants infected with the indicated viruses.  
784 Each bar represents the average of three plants (error bar = 1 standard deviation). For  
785 normalization, the average of wild type UCBSV is equal to 1. (E) Representative  
786 pictures of upper non-inoculated leaves, taken at 60 days post-inoculation, of cassava  
787 plants inoculated with the indicated viruses. White bar = 4 cm. (F) Analysis by agarose  
788 gel electrophoresis of a fragment of the UCBSV genome (V) and of a plant  
789 housekeeping gene (H) amplified by RT-PCR. RNA samples from upper non-  
790 inoculated leaves of 3 independent cassava plants inoculated with the indicated viruses  
791 were used as template.

792

793 **Figure 4. High accumulation of non-canonical nucleotides in cassava.** Base peak  
794 chromatogram in arbitrary units (AU) for representative samples of total NTPs

795 from *Manihot esculenta* (blue) and *Nicotiana benthamiana* (orange). The *M.*  
796 *esculenta*/*N. benthamiana* ratios for the average concentration (n=12 per plant species)  
797 of each NTP are indicated in parentheses. Non-canonical nucleotides are highlighted in  
798 red.

799

800 **Figure 5. Suboptimal separation of Nib-HAM1 during UCBSV infection.** (A)

801 Schematic representation of a NIaPro cleavage site. Substrate residues at both sides of  
802 the scissile bond are labeled by following a previously proposed nomenclature  
803 (Schechter and Berger, 1967). The consensus sequence of NIaPro substrates, as well as  
804 those residues present at the Nib-HAM1 junction in UCBSV, CBSV and EuRV, are  
805 indicated. The non-conserved residue at the Nib-HAM1 cleavage site of each virus is  
806 surrounded by a blue circle. (B) Schematic representation of the Nib-to-CP genomic  
807 segment of viruses used in these experiments. Amino acids around the NIaPro cleavage  
808 sites are depicted. (C) Representative pictures of infected and non-treated *N.*  
809 *benthamiana* plants taken at 13 days post-inoculation. White bar = 4 cm. (D and E)  
810 Detection of Myc-tagged HAM1 and CP by immunoblot analysis in samples from upper  
811 non-inoculated leaves of *N. benthamiana* plants infected with the indicated viruses. The  
812 positions of prestained molecular mass markers (in kilodaltons) run in the same gels are  
813 indicated to the right. The black asterisk indicates the presence of a cross-reacting band  
814 in all the samples, including the untreated control. Blots stained with *Ponceau* red  
815 showing the large subunit of the ribulose-1,5-bisphosphate carboxylase-oxygenase are  
816 included as a loading control.

817

818 **Figure 6. UCBSV HAM1<sub>TIA</sub> mutant, which undergoes an optimal cleavage at the**

819 **Nib-HAM1 junction, evolves to display partial split.** (A) Representative pictures of

820 upper non-inoculated leaves, taken at 60 days post-inoculation, of cassava plants  
821 inoculated with the indicated 2xMyc-tagged versions of UCBSV. White bar = 4 cm. (B)  
822 Analysis by agarose gel electrophoresis of a fragment of the UCBSV genome (V) and a  
823 plant housekeeping gene (H) amplified by RT-PCR. RNA samples from upper non-  
824 inoculated leaves of 3 independent cassava plants inoculated with the indicated viruses  
825 and collected at 60 dpi, were used as template. (C) Chromatograms of Sanger  
826 sequencing results of the UCBSV genomic fragment of interest amplified by RT-PCR.  
827 RNA samples from upper non-inoculated leaves of a cassava plant inoculated with the  
828 UCBSV-HAM1<sub>TIA</sub>-2xMyc mutant were used as template. Leaves for RNA preparation

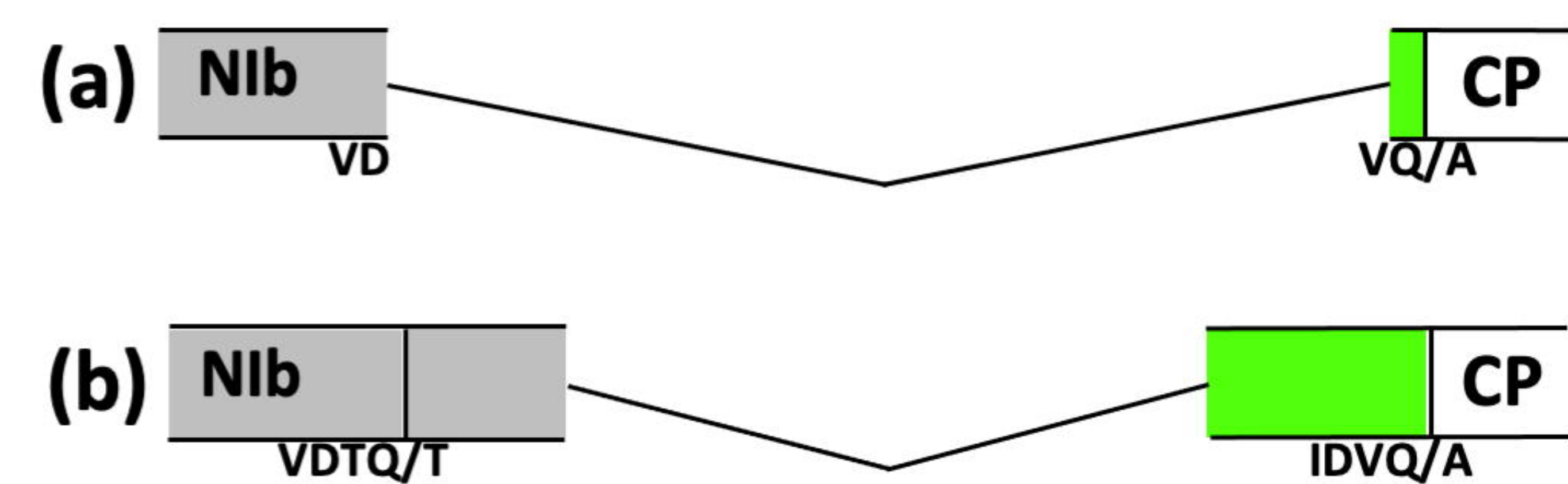
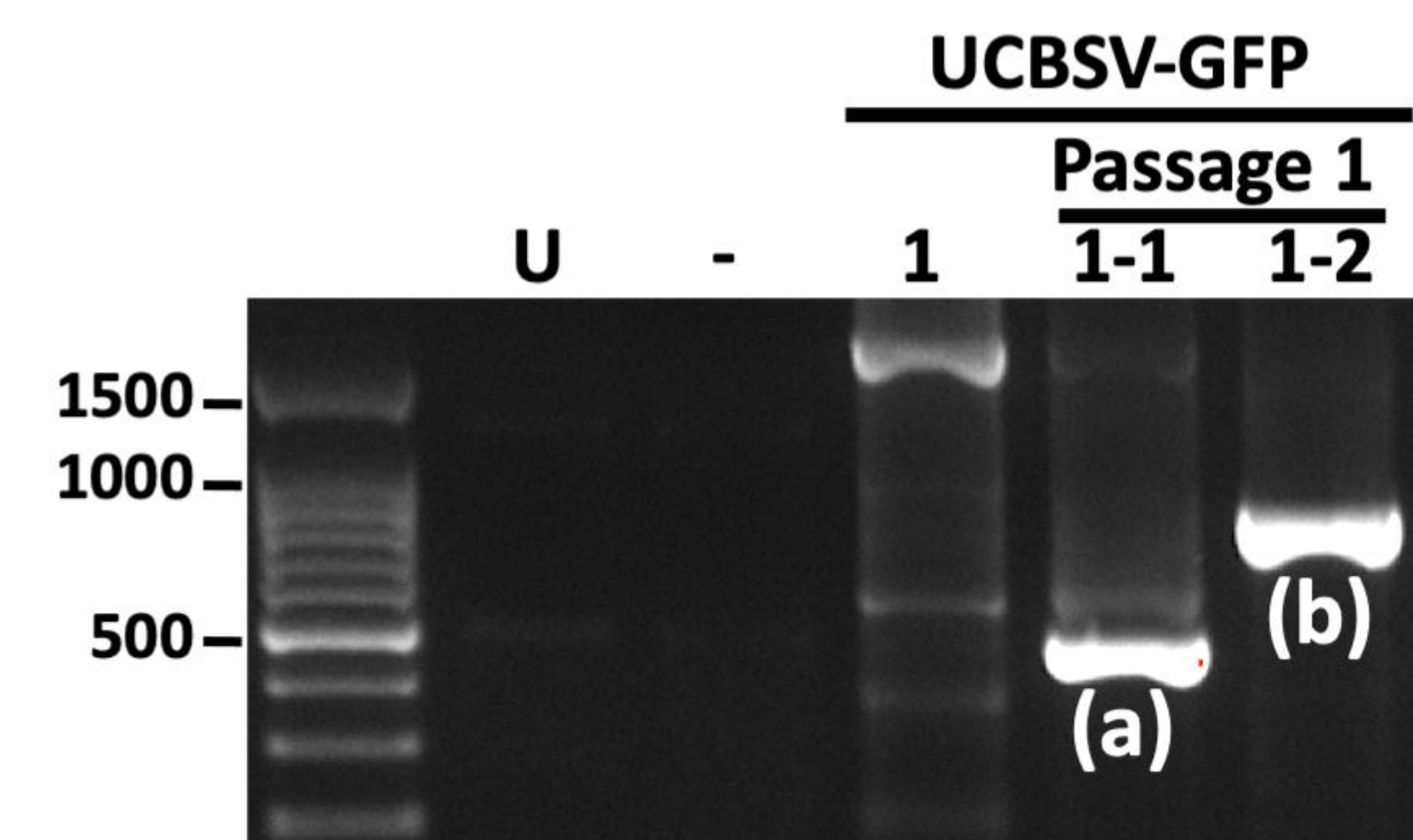
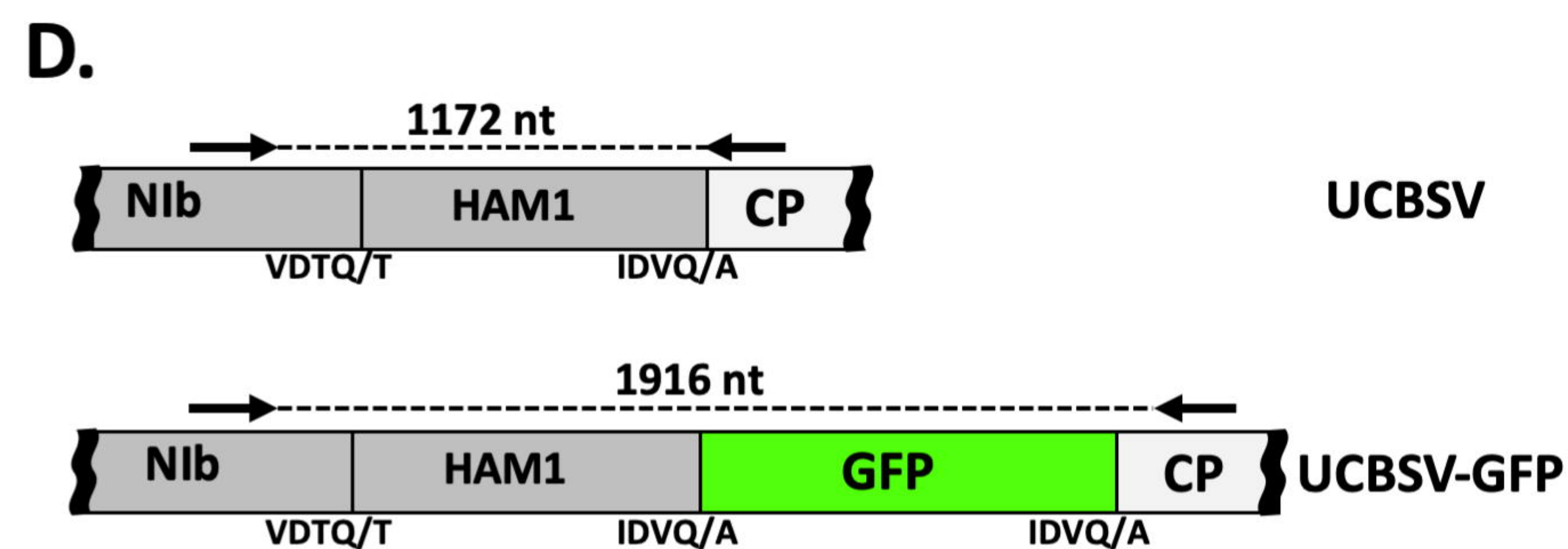
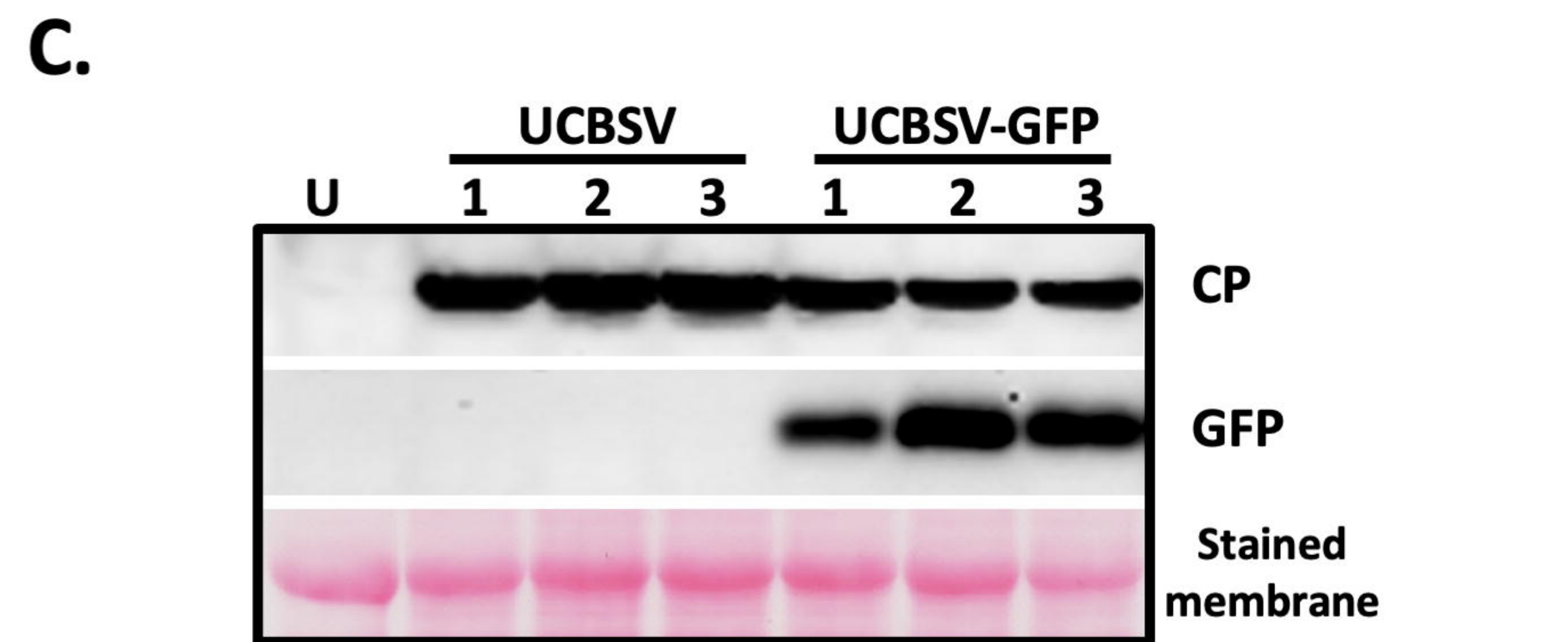
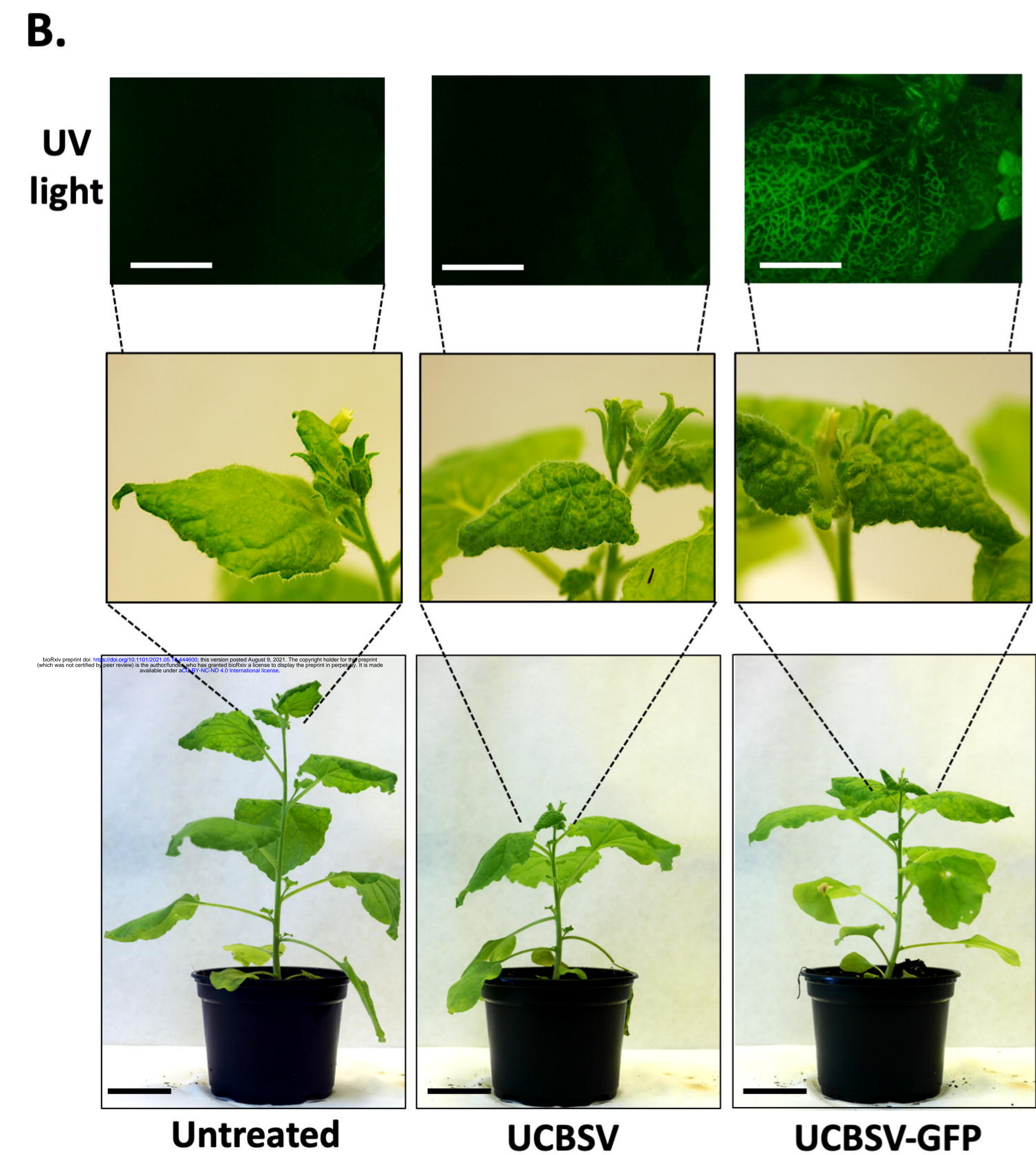
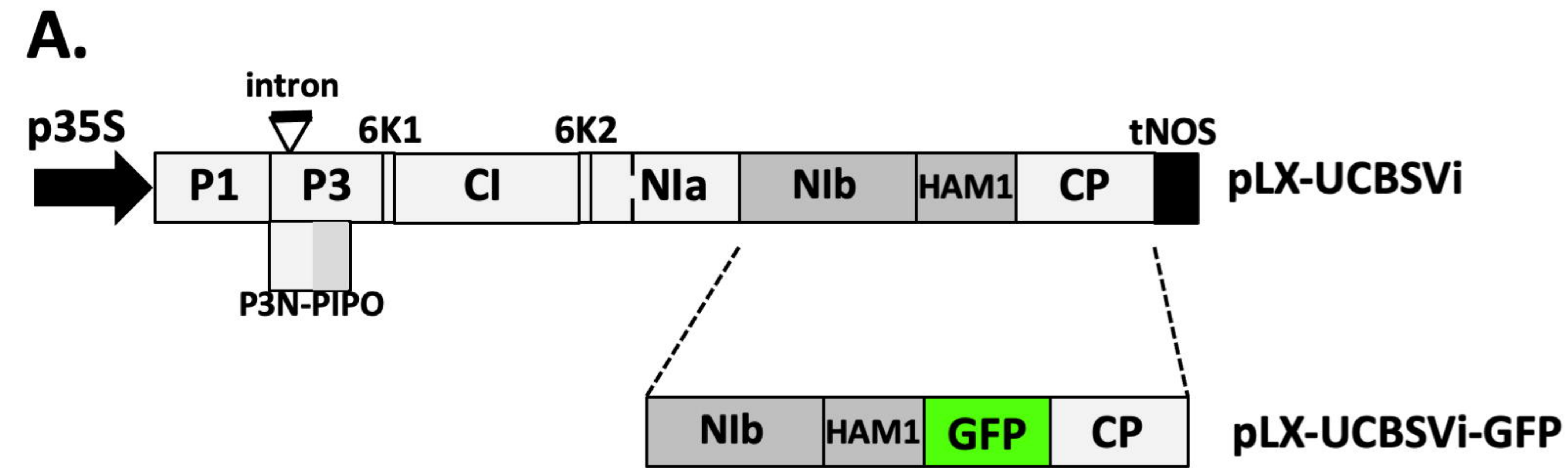
829 were harvested at 60 and 180 dpi. Residues derived from the original mutation and from  
830 the spontaneous second mutation are surrounded by a red circle. (D) Detection of Myc-  
831 tagged HAM1 and UCBSV CP by immunoblot analysis in samples from upper non-  
832 inoculated leaves of *N. benthamiana* plants infected with the indicated viruses. The  
833 positions of prestained molecular mass markers (in kilodaltons) run in the same gel is  
834 indicated to the right. Blot stained with Ponceau red showing the large subunit of the  
835 ribulose-1,5-bisphosphate carboxylase-oxygenase is included at the bottom as a loading  
836 control.

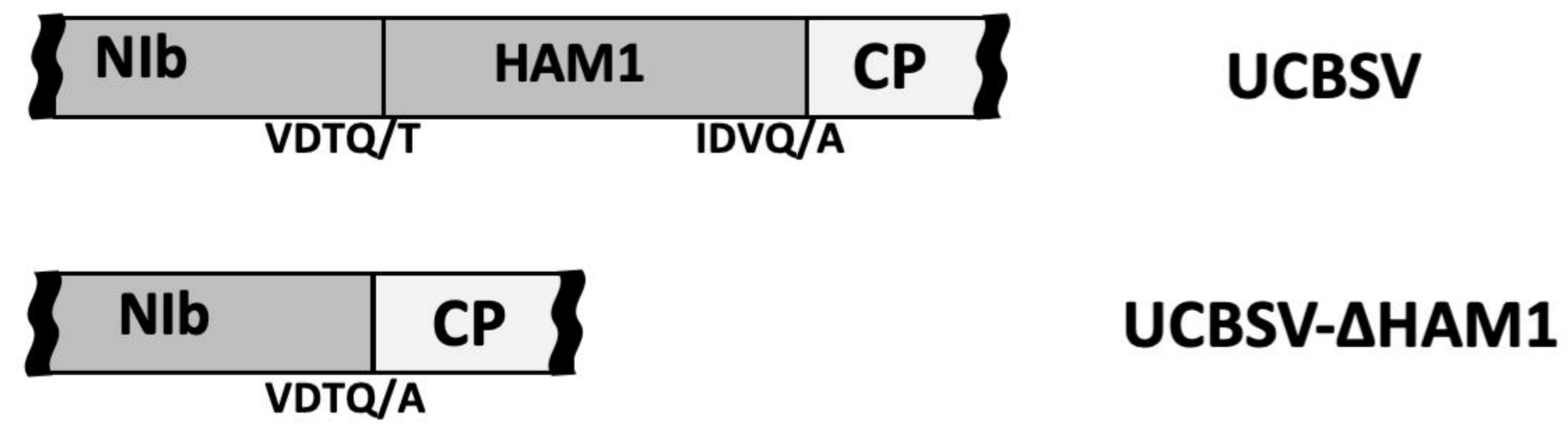
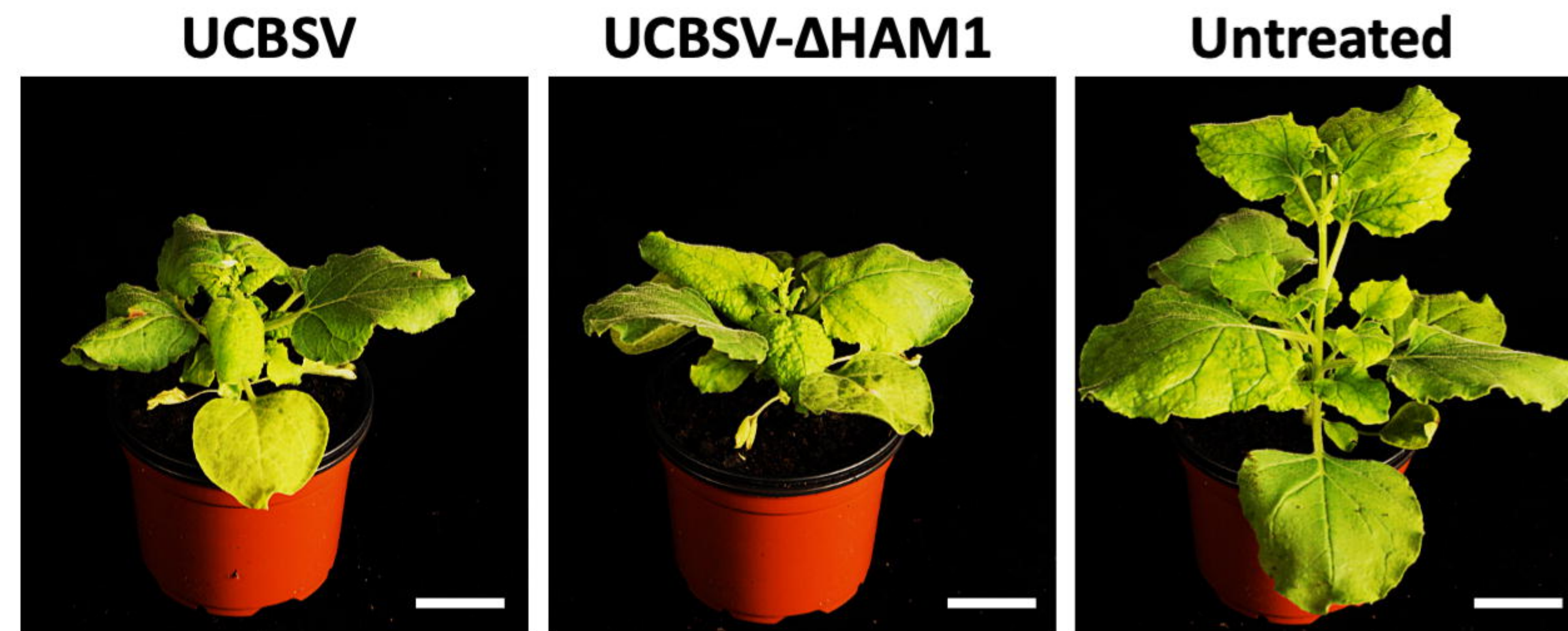
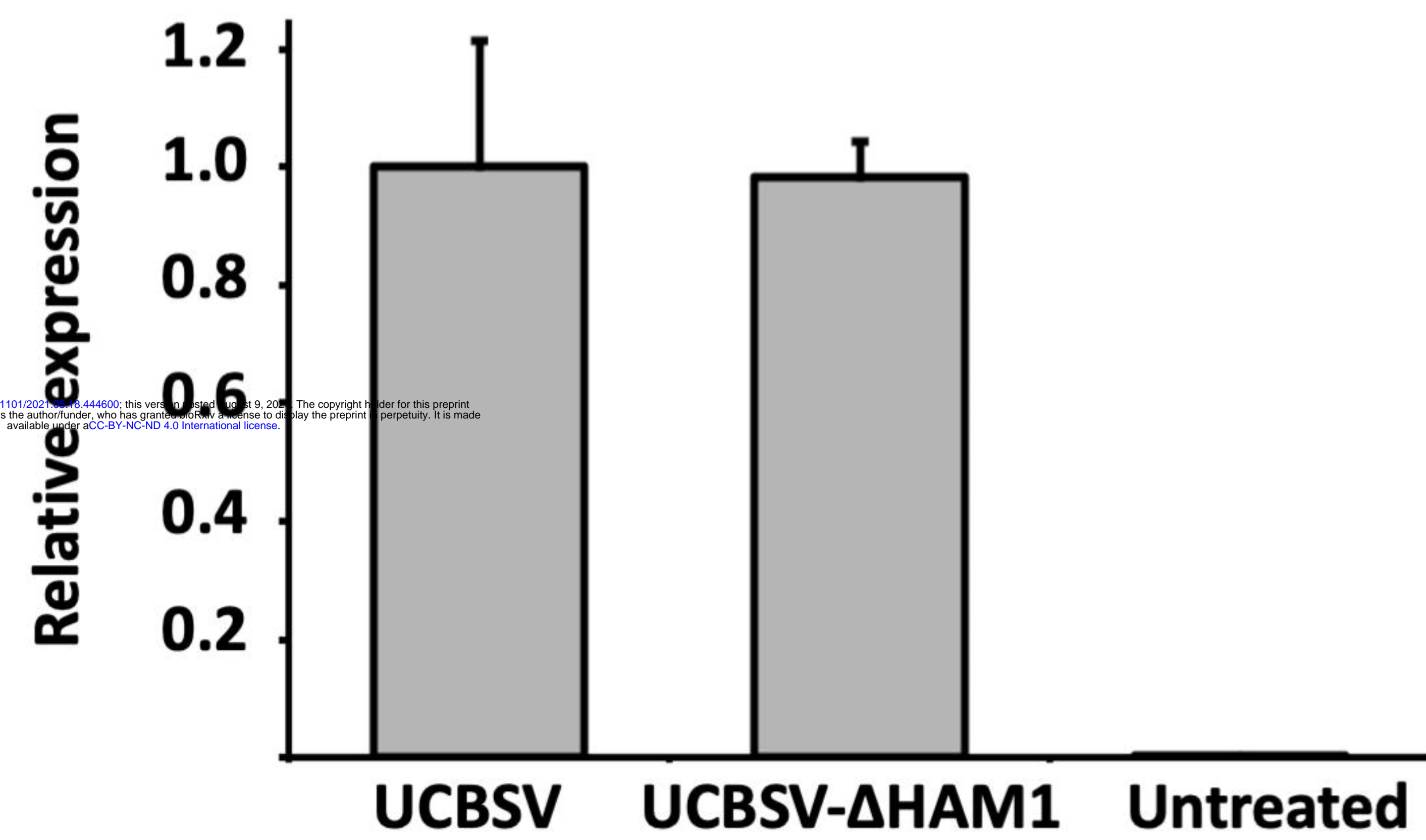
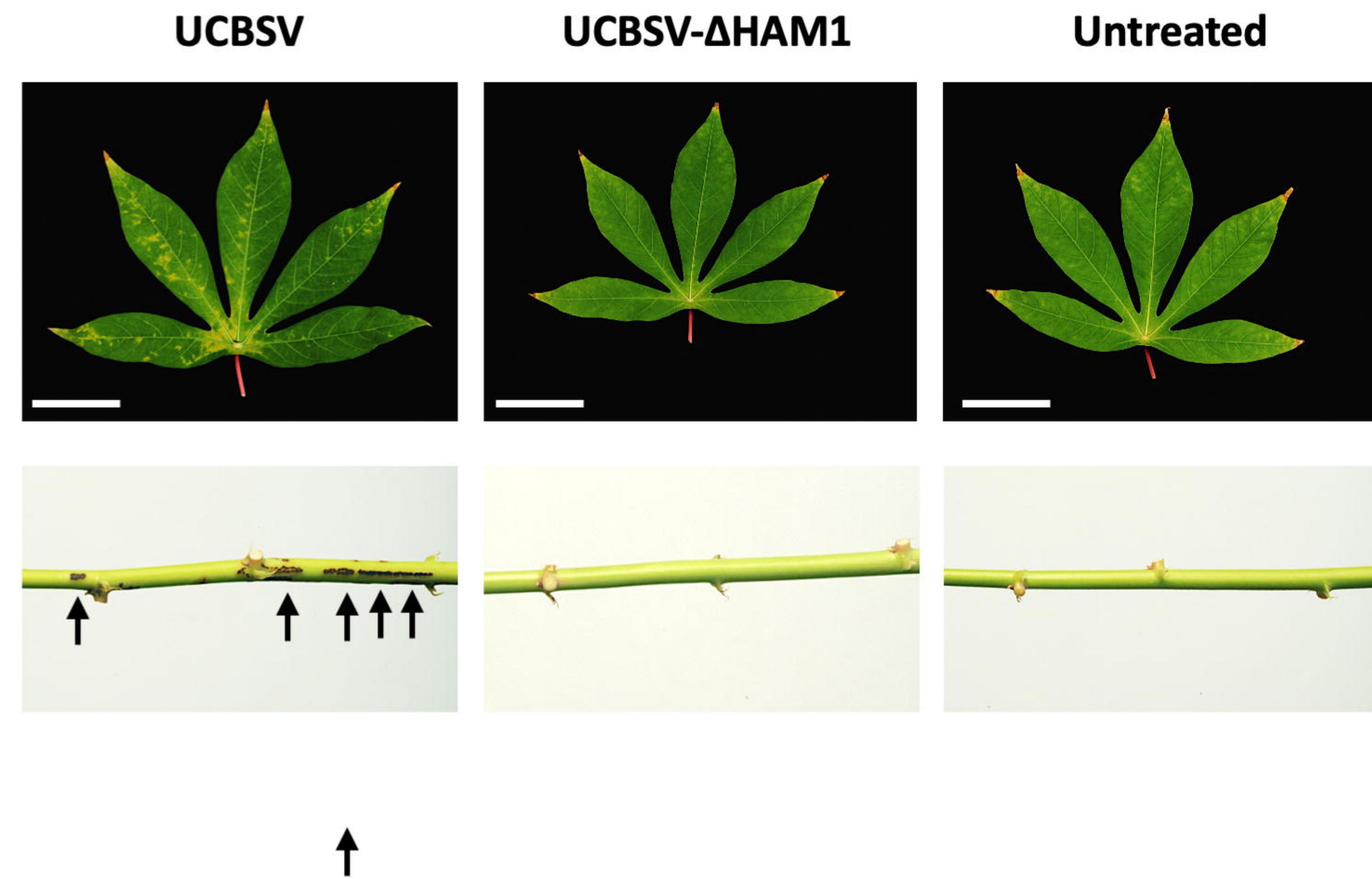
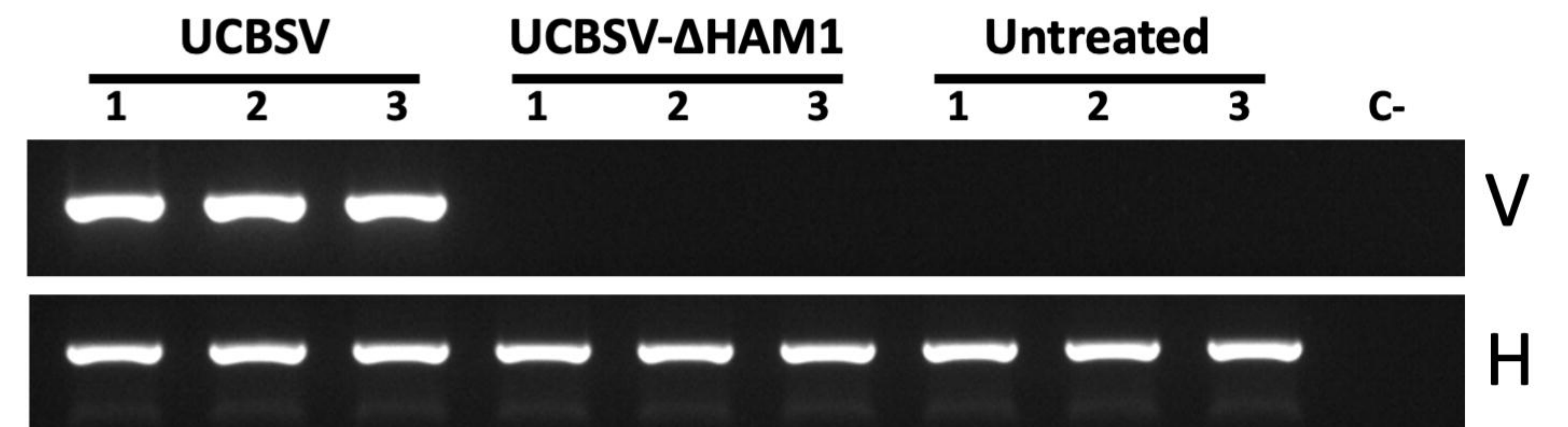
837

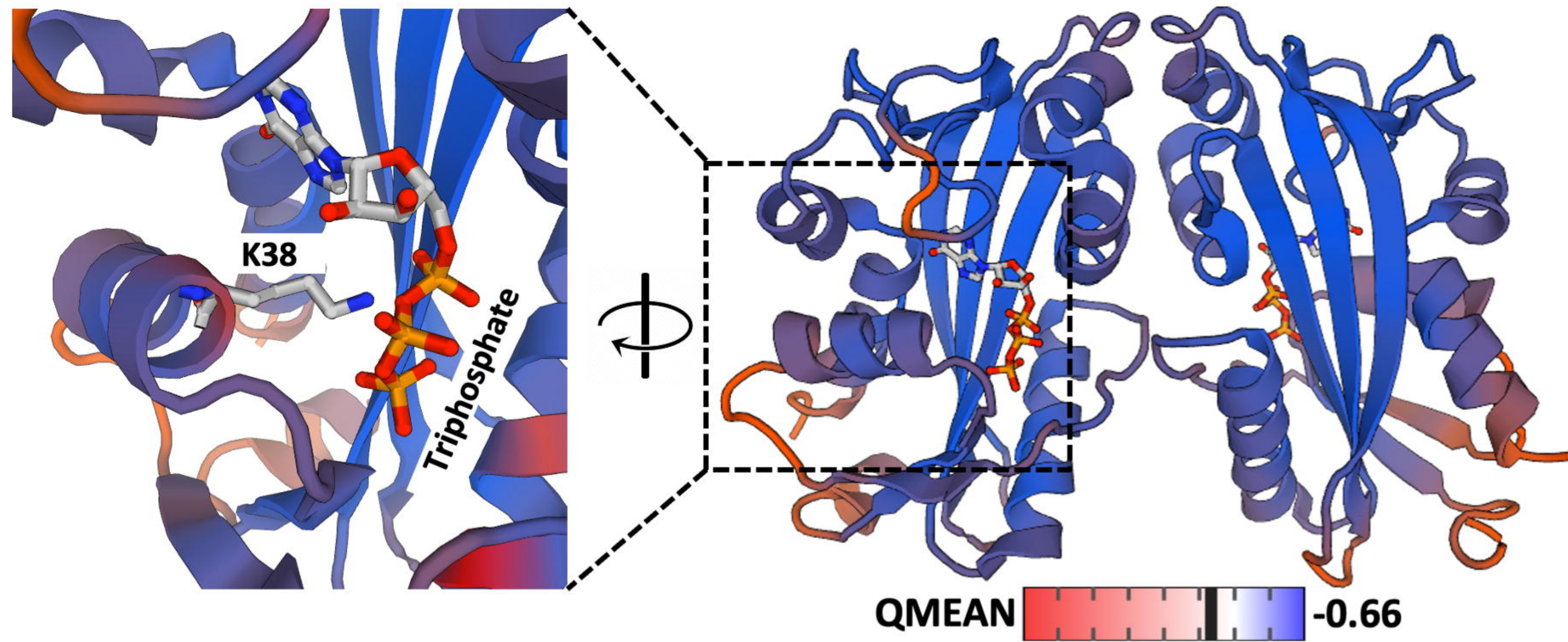
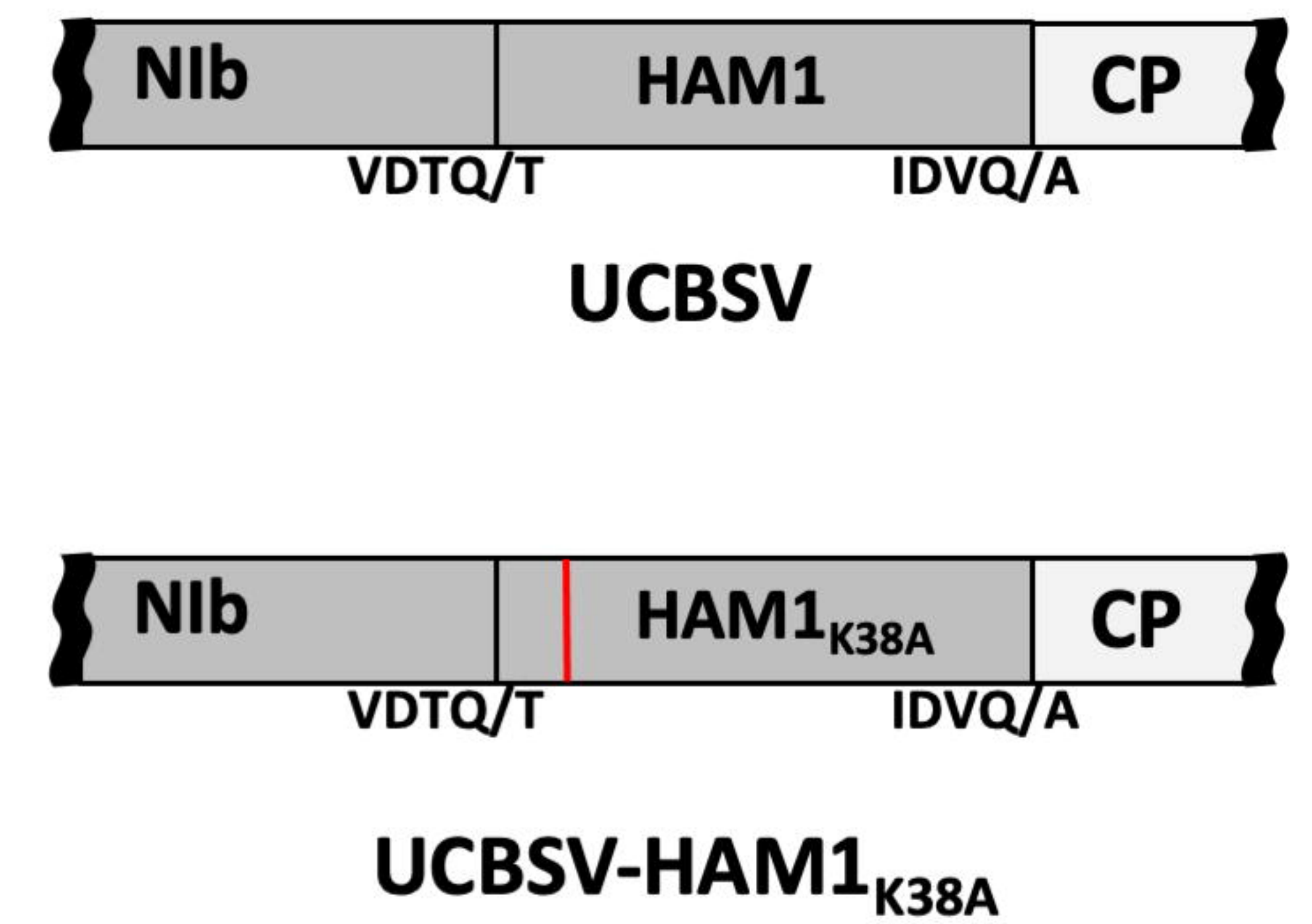
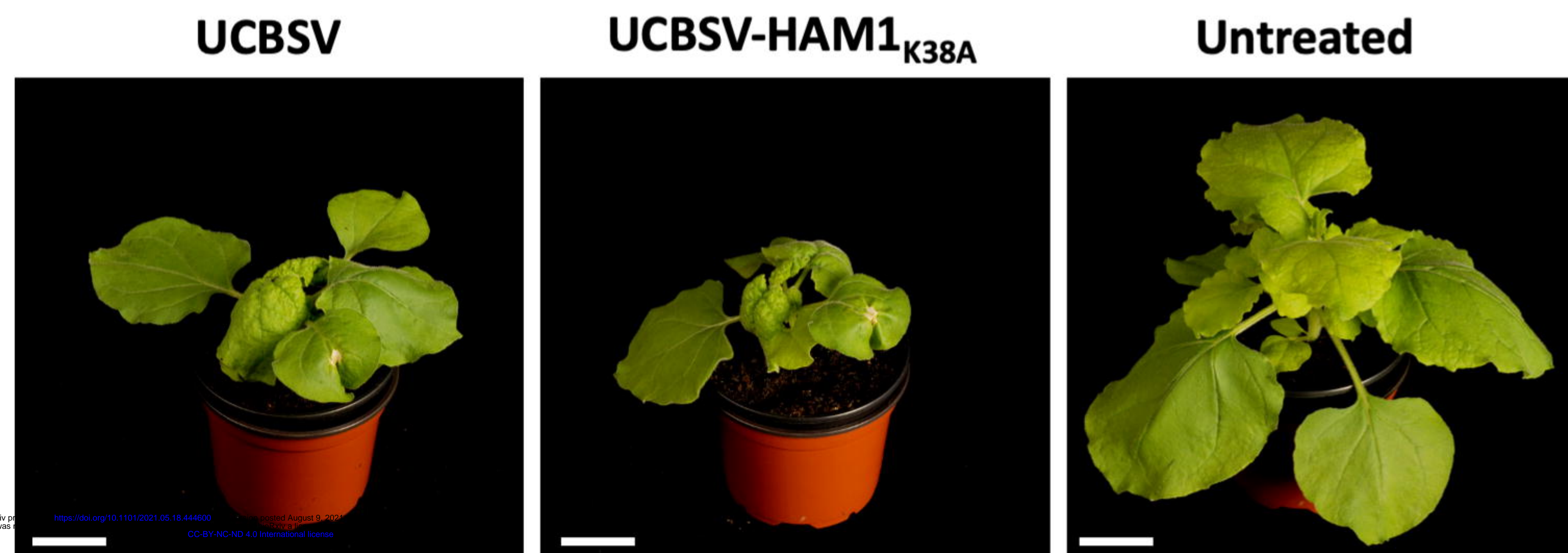
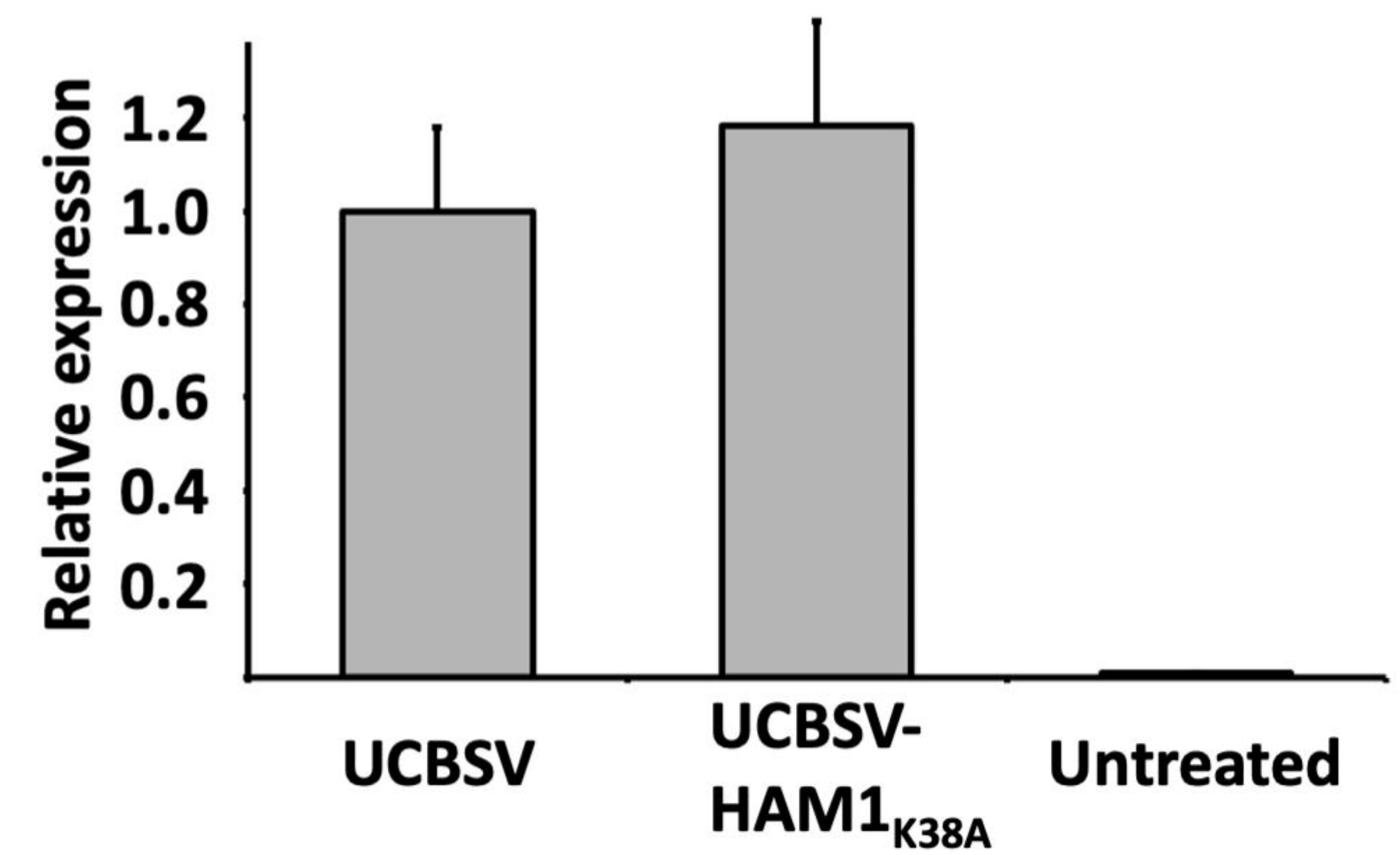
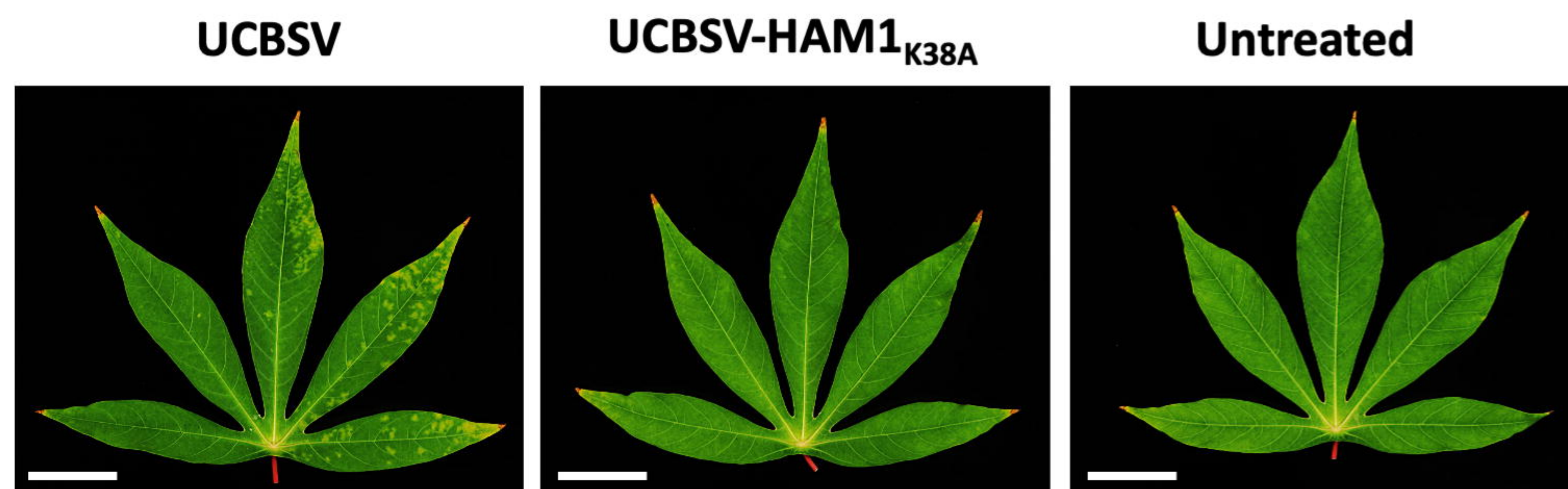
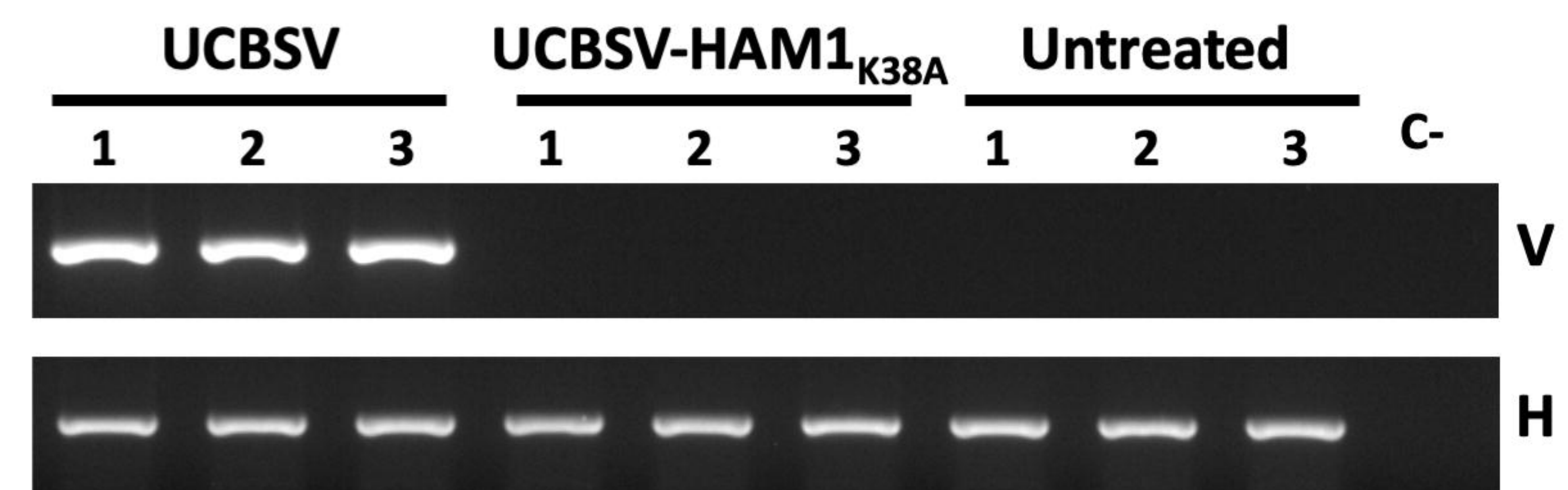
838 **Figure 7. Suboptimal split of Nib-HAM1 is a general feature of potyvirids.**

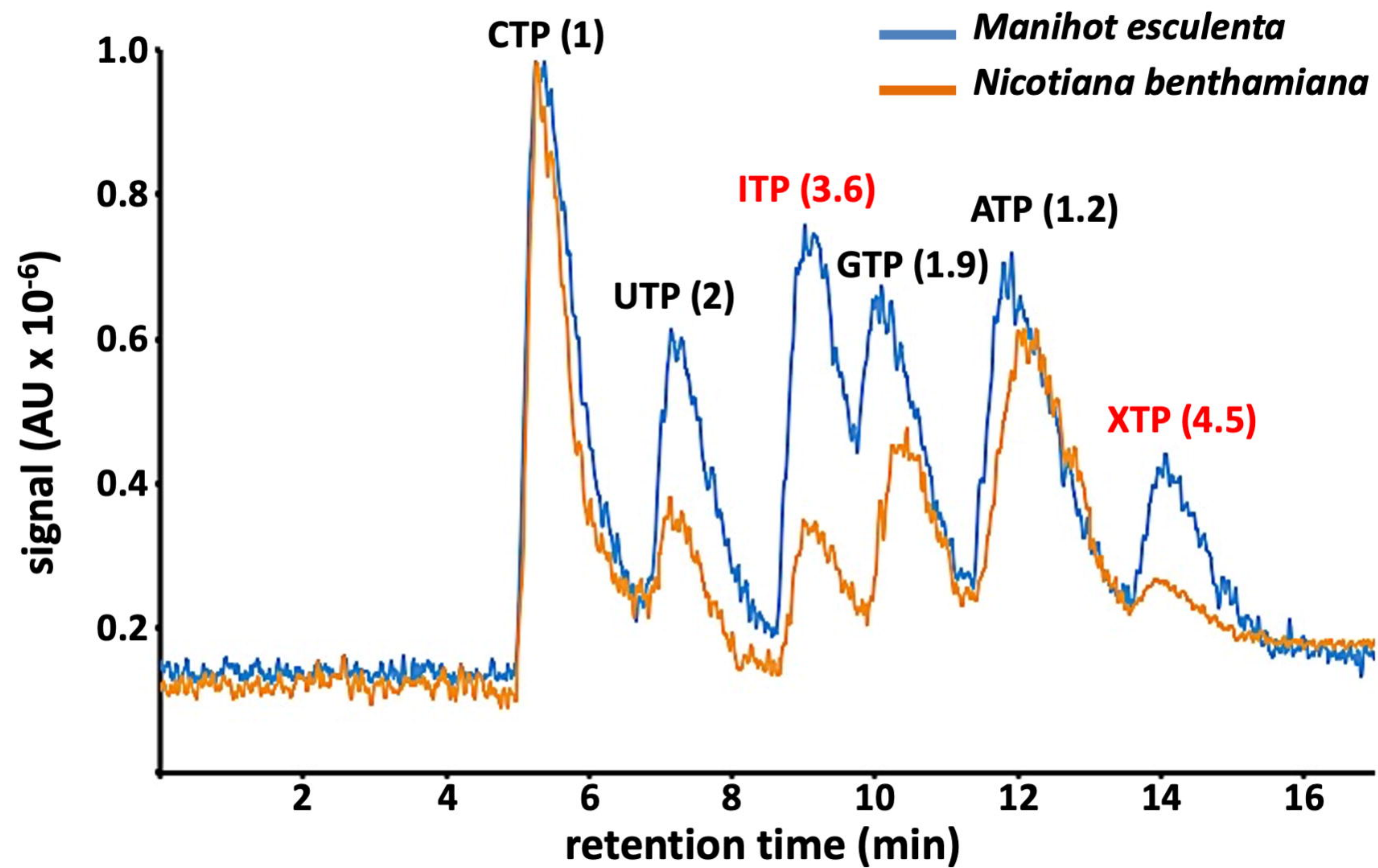
839 Schematic representation of constructs based on pGWB702 $\Omega$  and pGWB718 (Tanaka et  
840 al., 2011) used for these experiments. p35S: 35S promoter from cauliflower mosaic  
841 virus; tNOS: terminator from the NOS gene of *Agrobacterium tumefaciens*; Nib<sub>C</sub>: Nib  
842 C-terminus; CP<sub>N</sub>: CP N-terminus. (B) Detection of Myc-tagged proteins by immunoblot  
843 analysis in samples from *N. benthamiana* leaves expressing Nib<sub>C</sub>-HAM1-CP<sub>N</sub> versions  
844 in either the absence (-) or presence (+) of their cognate NIa. Viruses from which the  
845 transiently expressed proteins derived are indicated. Blots stained with Ponceau red  
846 showing the large subunit of the ribulose-1,5-bisphosphate carboxylase-oxygenase are  
847 included at the bottom as a loading control.



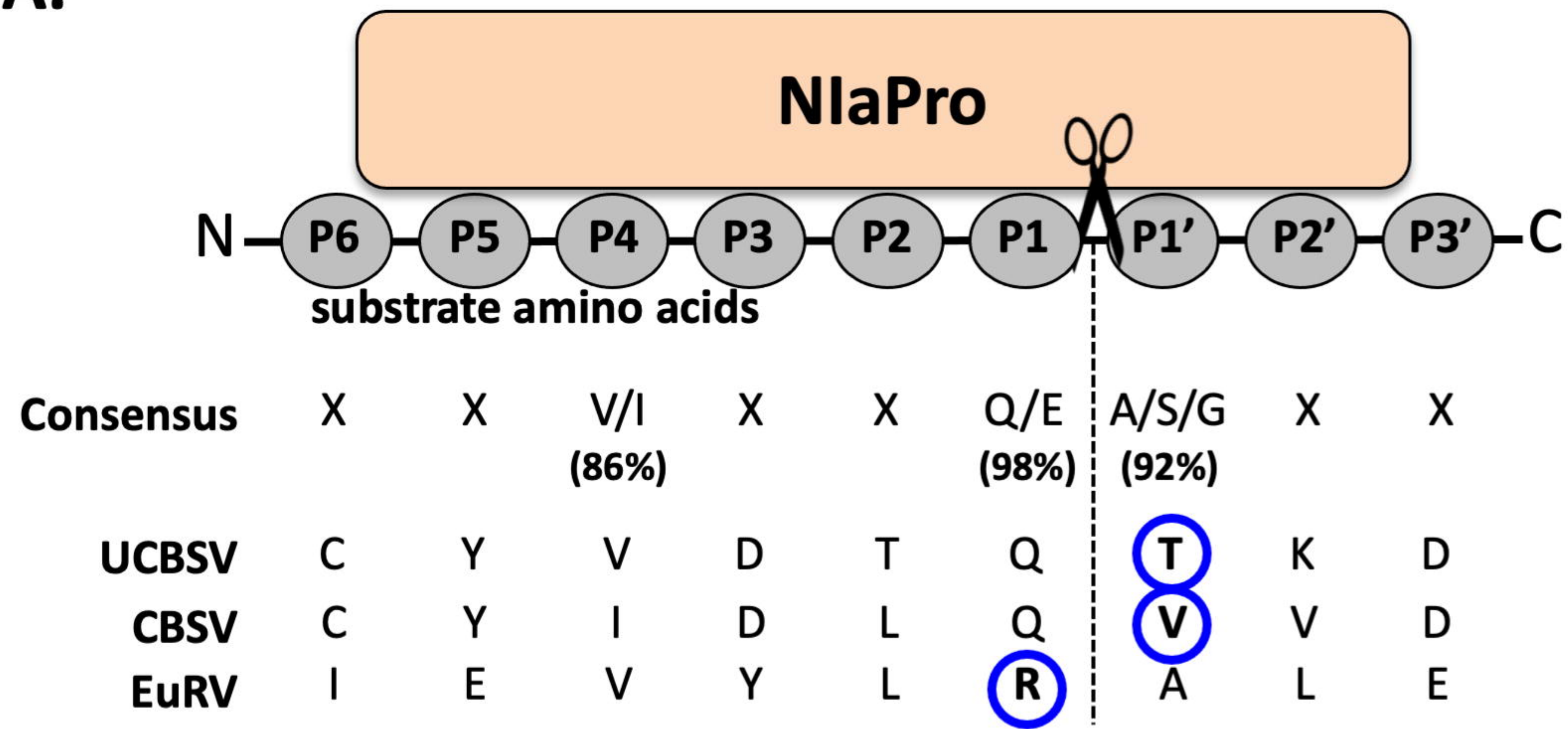


**A.****B.****C.****D.****E.**

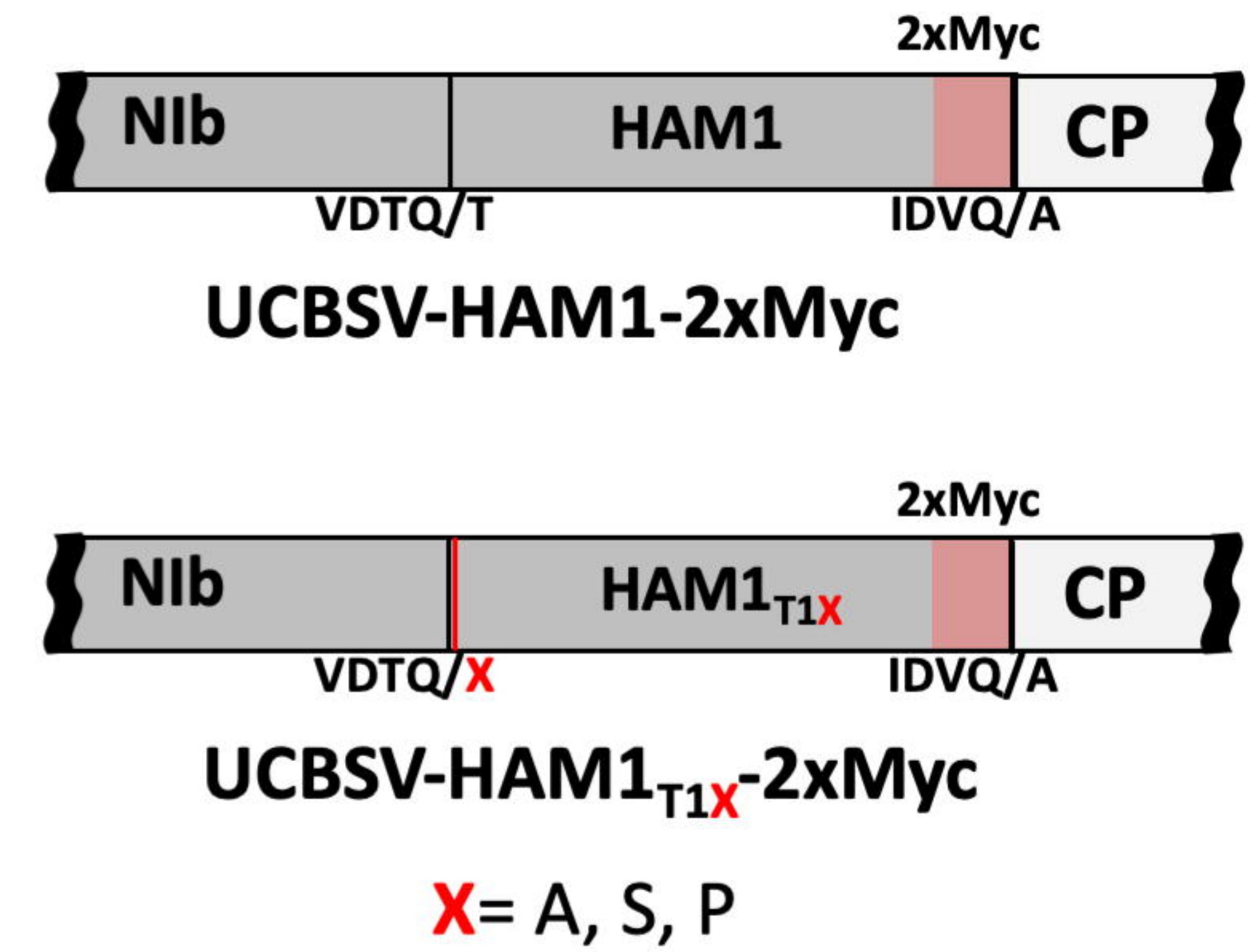
**A.****B.****C.****D.****E.****F.**



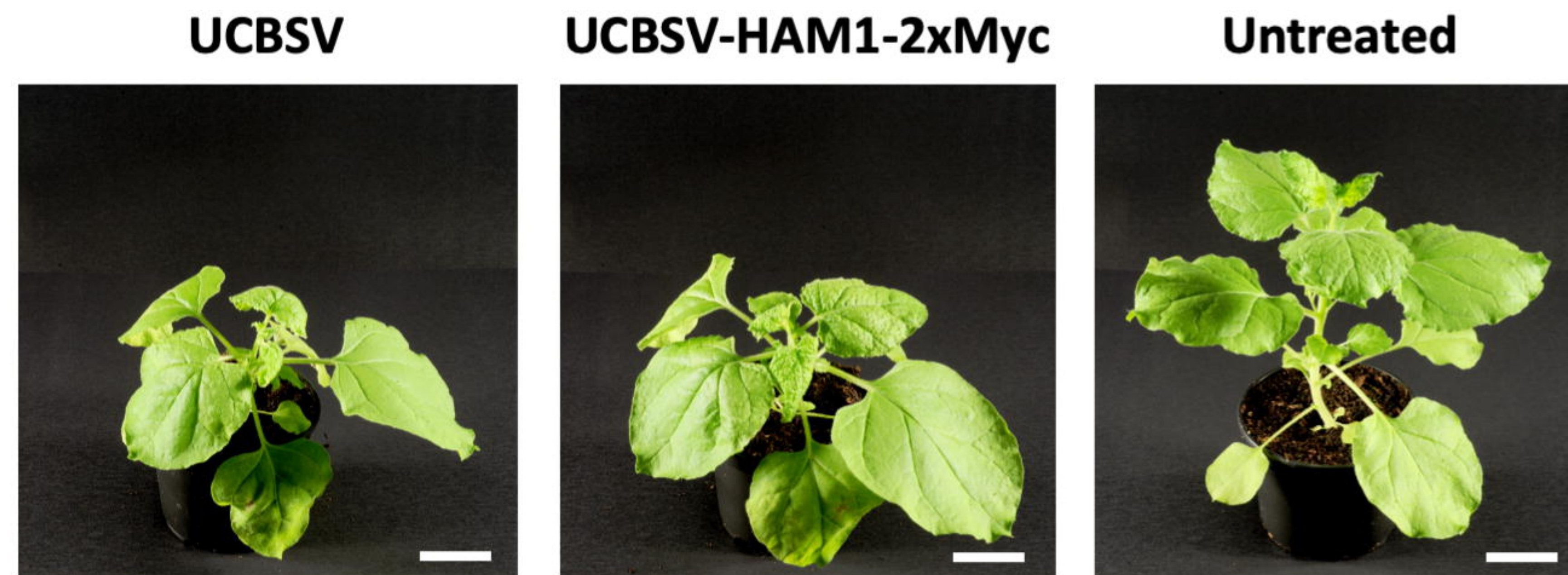
**A.**



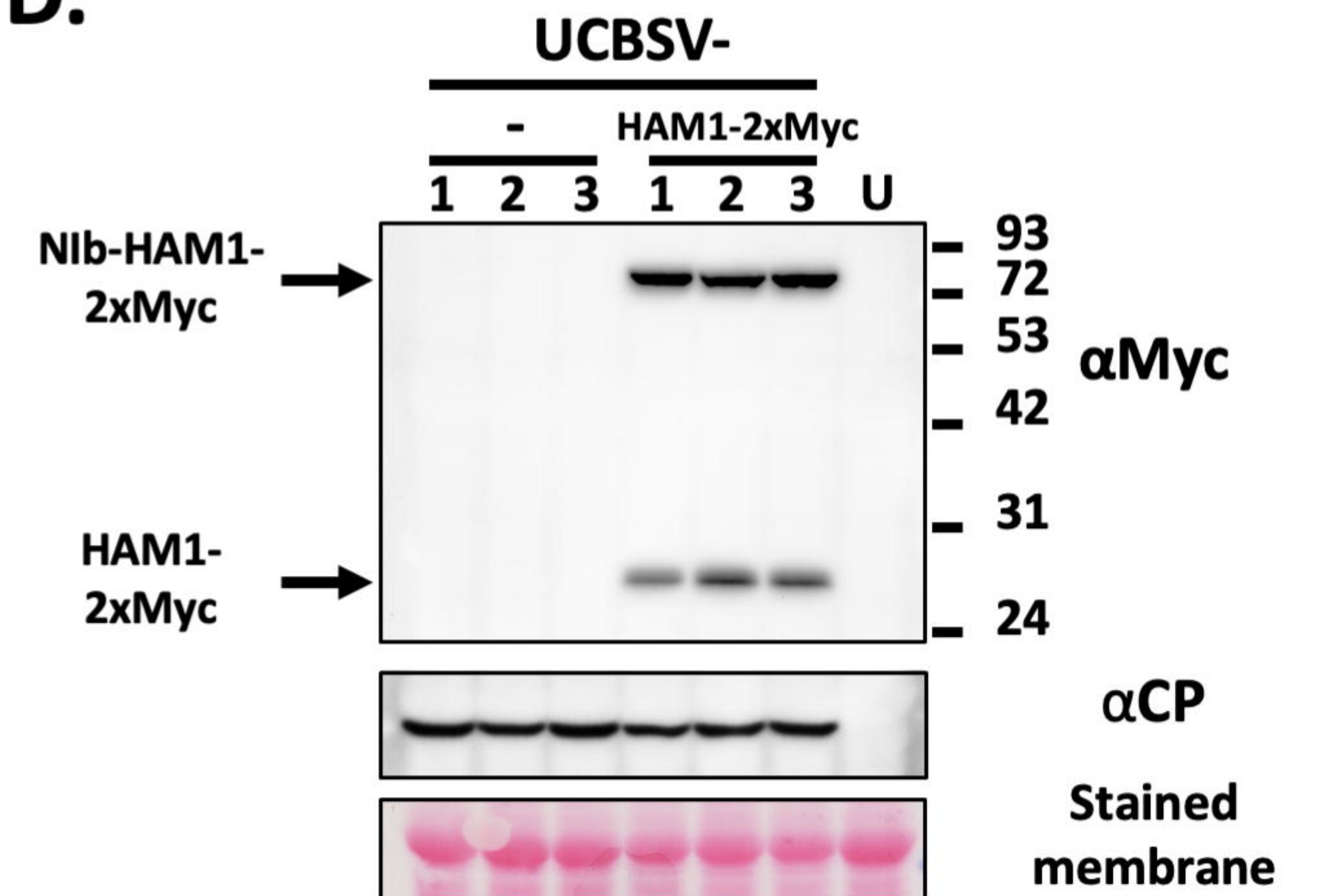
**B.**



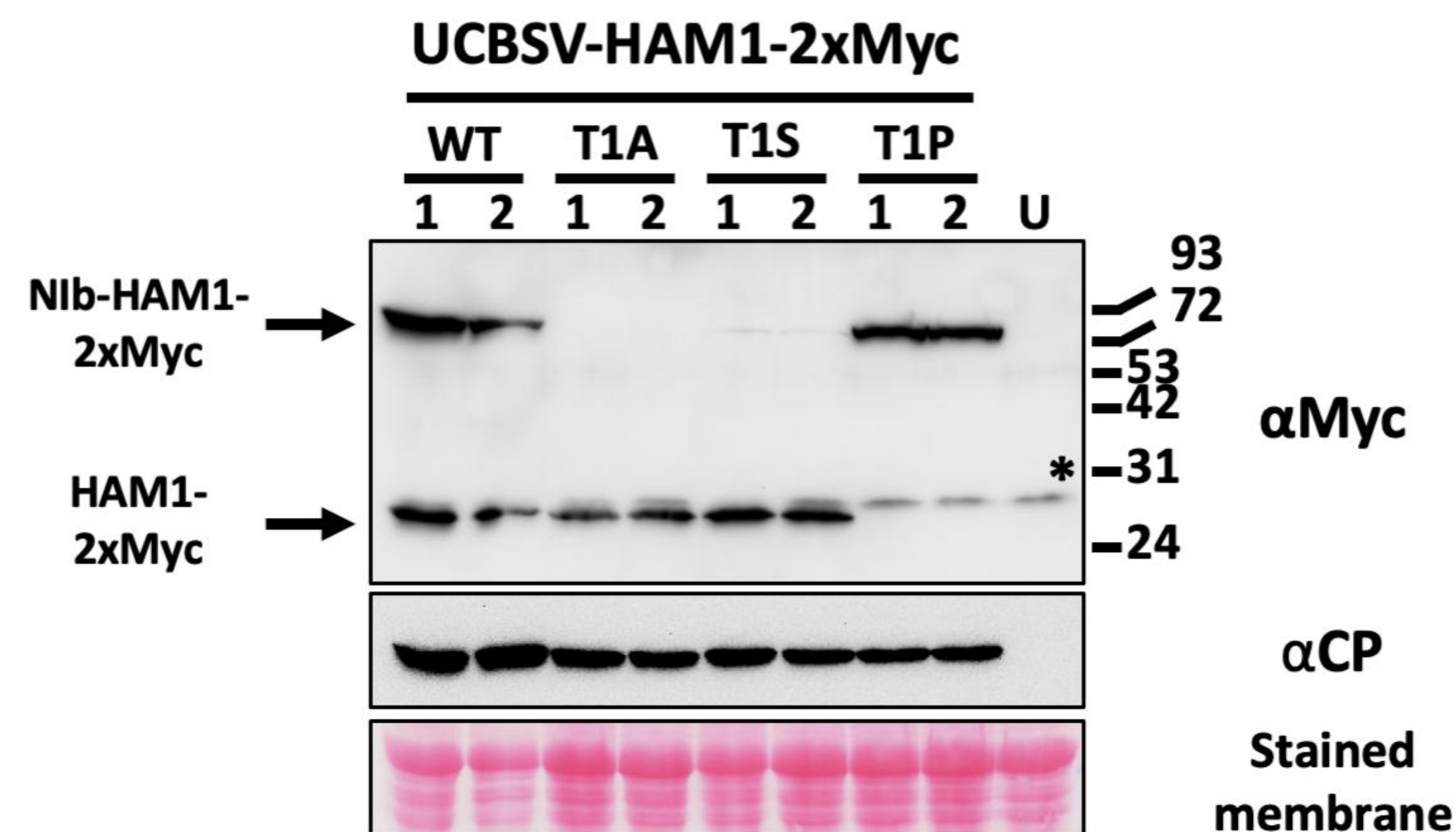
**C.**

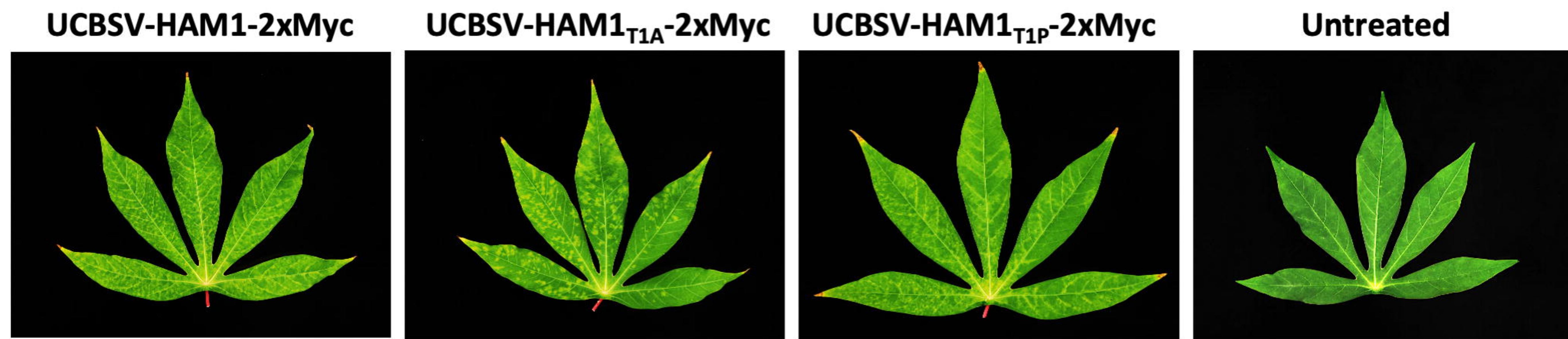
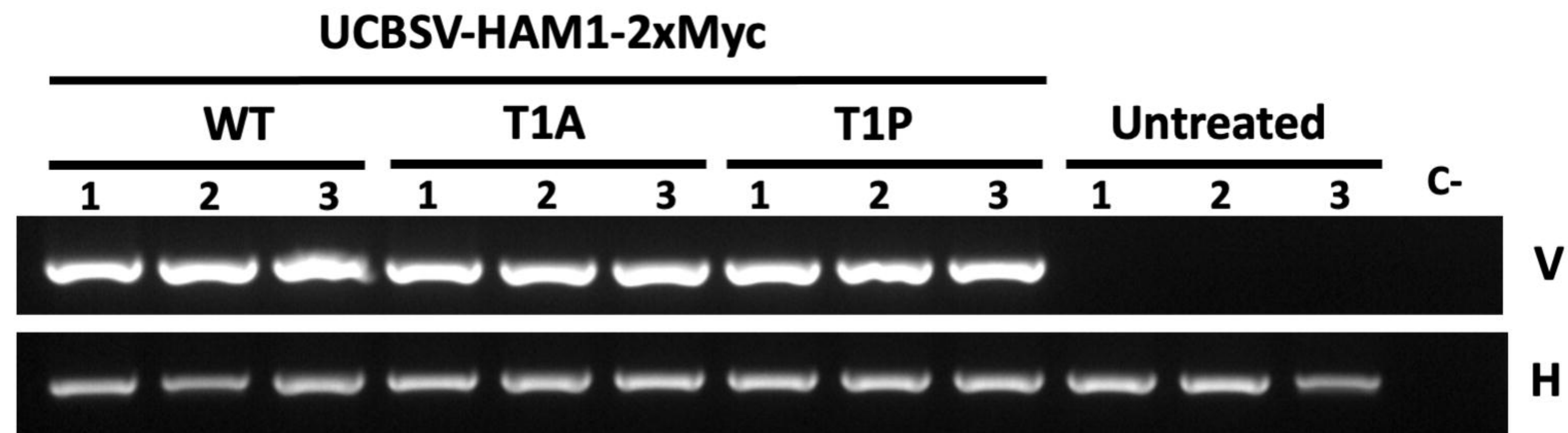


**D.**

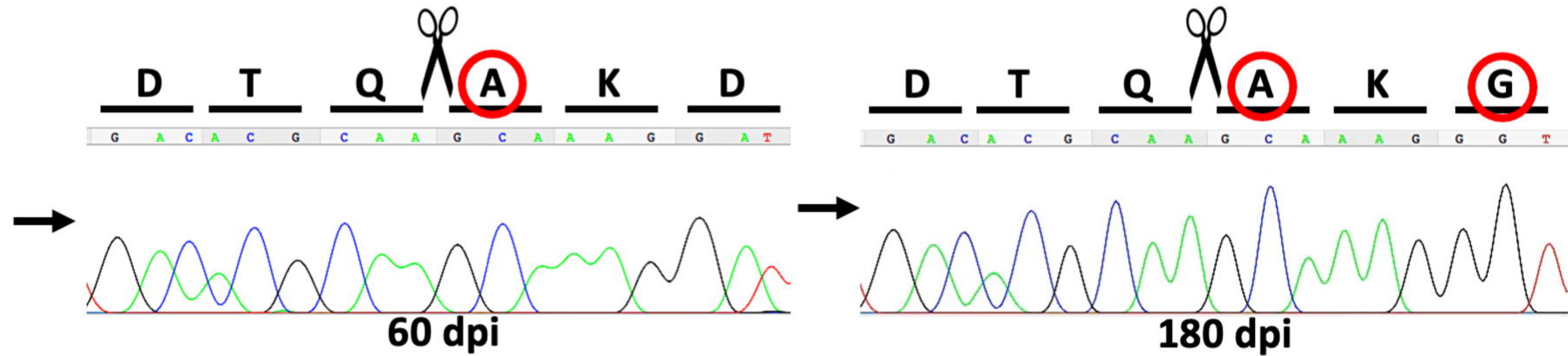
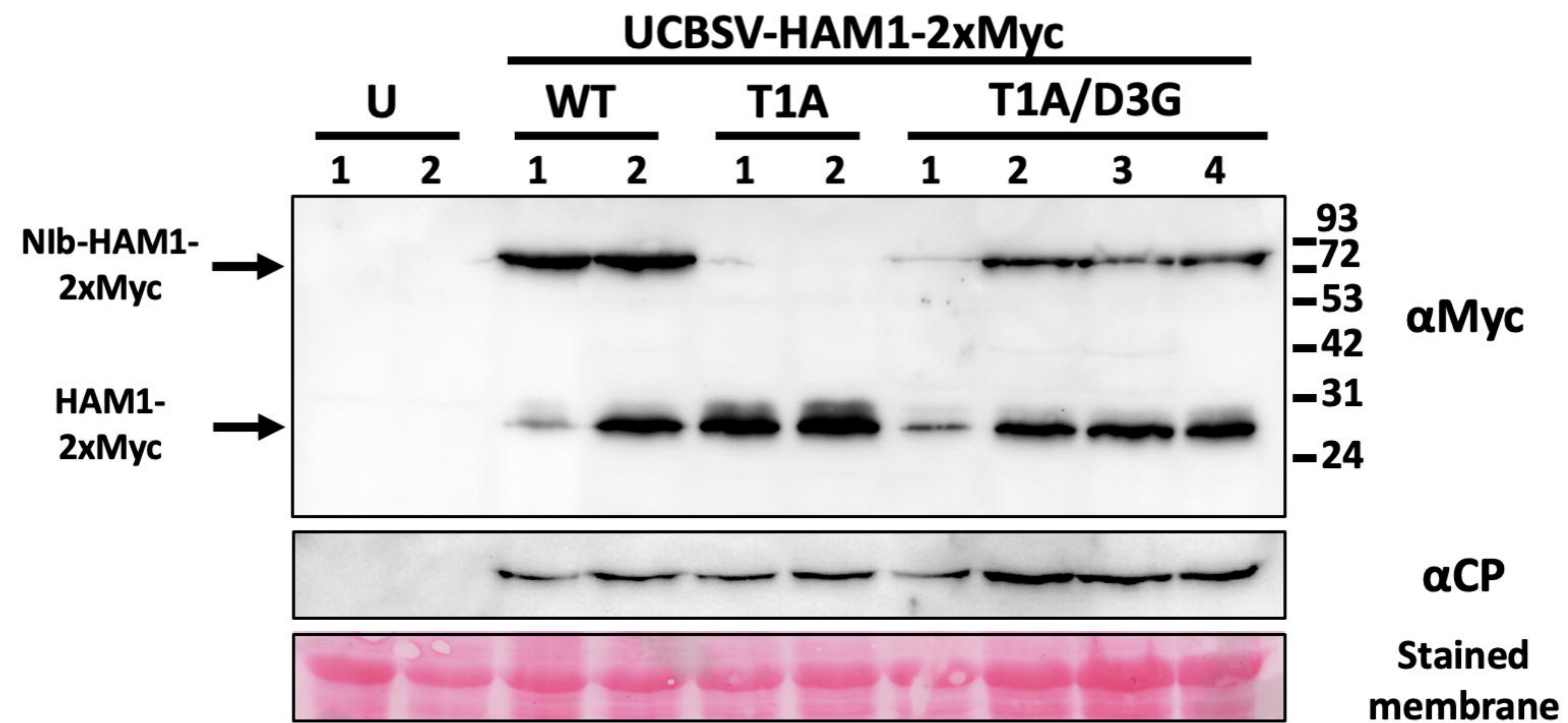


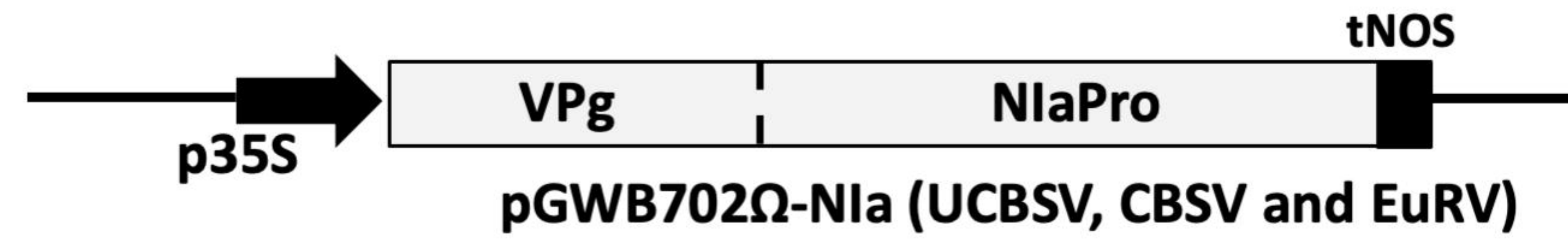
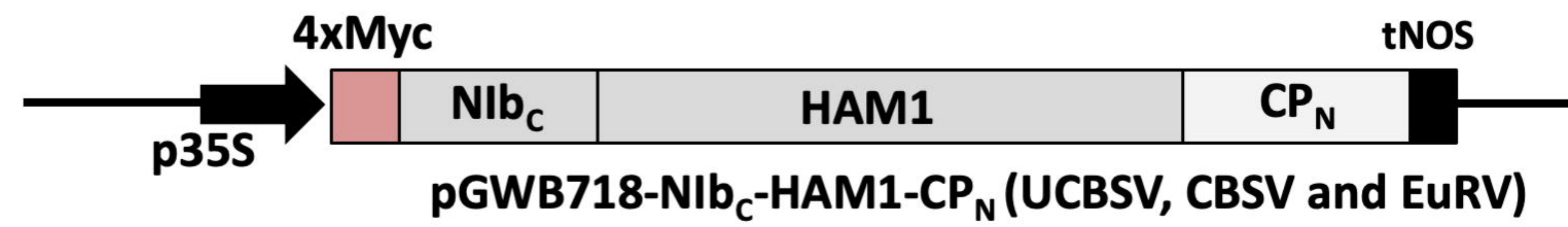
**E.**



**A.****B.****C.**

UCBSV-HAM1<sub>T1A</sub><sup>-</sup>  
2xMyc

**D.**

**A.****B.**